Multiscale Modeling with Extended Bridging Domain Method*

Mei Xu, Robert Gracie, and Ted Belytschko
Northwestern University
2145 Sherman Ave, Evanston, IL, 60208

1 Introduction

This Chapter describes the concurrent coupling of atomistic methods with continuum mechanics. Such models are useful in the study of phenomena such as fracture and dislocation dynamics, where molecular mechanics and/or quantum mechanics models are required for phenomena such as bond breaking, but the relevant configuration is far too large to permit a completely atomic description. To make such problems computationally tractable, the quantum/atomistic model must be limited to small clusters of atoms in the vicinity of a domain of interest where such high resolution models are necessary and a continuum method should be used for the rest of the domain, see e.g. Khare et al. [1, 2]. In the remainder of the domain, where no bond breaking occurs, the continuum description permits much less expensive computations with sufficient accuracy to describe the behavior of the system.

This chapter describes two types of concurrent models

1. mechanical equilibrium models
2. molecular dynamics models

Equilibrium models are used to determine the energy landscape of a system, i.e. the surface that gives the energy at 0 K. They provide valuable information about the system such as energy differences due to configurational changes, activation barriers, etc. The adjective *mechanical* should be carefully noted. Equilibrium is often used in molecular mechanics to describe thermodynamic equilibrium in atomistic systems, but thermodynamic equilibrium pertains only to molecular dynamics and is distinct from mechanical equilibrium. Mechanical equilibrium can be thought of as molecular statics, in contrast to molecular dynamics.

We will describe five concurrent coupling methods

1. direct and master-slave coupling
2. the ONIOM method
3. the bridging domain method
4. the quasicontinuum method
5. the bridging scale method

Although this list is not comprehensive, it provides a birdseye view of concurrent methods. We will first give a brief review of the literature. This is followed by a taxonomy of multiscale methods, so that the place of concurrent methods can be seen. Several concurrent methods are then described. Similarities and differences of the methods will be described, along with their advantages and disadvantages. The description is by no means comprehensive and emphasizes the bridging domain method.

Among the first atomistic/continuum models are those in Baskes et al.[3] and Mullins and Dokainish [4]. The latter studied a plane crack in alpha iron. In their model, the finite element mesh was coarser than the lattice constant (note: the lattice constant is the distance between nuclei). The displacements of the atoms not coincident with finite

*Chapter in *Bridging the Scales in Science and Engineering*, edited by J. Fish, Oxford Press.

element nodes were prescribed by using the finite element interpolation (the term nuclei is more precise since atoms include the electrons, but we will use both interchangeably). It can be said that the atoms were slaved to the finite element mesh. This procedure is often called a master-slave approach in the finite element literature, see Belytschko et al. [5], and we will use this nomenclature here and describe the method.

Kohlhoff et al. [6] similarly coupled finite elements with an atomistic model in a method called FEAt, but they used a nonlocal elasticity theory for the continuum in the overlapping domain to link with the nonlocal lattice theories. The model was applied to the cleavage fracture of two b.c.c. crystalline materials, tungsten and iron. The FEAt method introduces the concept of a “pad" which overlaps the finite element model. However, the energy of the underlying finite element model is not included in the total energy. Its purpose is to provide the displacements of the pad atoms. At the atomistic/finite element interface, the nodes and atoms are coincident to ensure the compatibility between the two models.

The quasicontinuum method (QC) (Tadmor, Ortiz and Phillips, [8]) is aimed at making the transition to atomistic more seamless. The entire model is viewed as an atomistic model; finite element interpolation and the Cauchy-Born rule are used to eliminate atoms where atomic resolution is not needed. Accurate computation of the energy in the *atomistic* subdomain requires that the atoms be coincident with the finite element nodes. Representative atoms are selected to define a subspace in order to eliminate the unnecessary atomistic degrees of freedom, and the mechanical variables, e.g. displacement and forces, of the atoms inside the elements of the subspace are calculated using finite element interpolation. This almost bypasses the distinction between atomistic and continuum domains. Ghost forces due to the mismatch in the transition zone were later taken care of by the developers of the method [9]. The convergence, accuracy and the effect of tolerances were evaluated in [10]. Several special purpose variants of the method have been developed. For example, Knap and Ortiz [10] formulated a cluster summation rule for the QC method, which made it possible to apply the QC model to more complex problems. Rudd and Broughton [11] developed a similar method, called the coarse-grained molecular dynamics (CGMD) method. The coincidence of the atoms and nodes was required and the equations of motion were directly obtained from a statistical coarse graining procedure.

Shilkrot et al. [7] developed the coupled atomistic/discrete-dislocation (CADD) method, which combines the QC method with continuum defect models. It added the capability to pass dislocations between the atomistic and the continuum model. Closed form solutions and superposition methods were used for this purpose, and the *pad* atoms were used in CAAD method too, but they were not slaved to the continuum nodes. The contribution of the *pad* was to eliminate the free surface when dealing with the atomistic model.

Considerable interest in multiscale methods has been aroused by the pioneering work of Abraham et al.[12] and Broughton et al.[13], in which a quantum model was added in the bond-breaking subdomain. Their method is called macroscopic-atomistic-ab initio dynamics (MAAD). In their atomistic/continuum coupling, the two models are overlapped and the contribution of each model to the total Hamiltonian is taken to be the average of the two Hamiltonians (i.e. the energies). The coupling procedure is only described briefly and appears to be rather ad hoc. They called the overlapping domain the *handshake* domain, and this name has become widely used. In their models, the finite element size at the atomistic/continuum interface was the same as the lattice constant.

Recently, several methods have been developed for equilibrium solutions and dynamics that do not require coincident nodes and atoms. Belytschko and Xiao [22] have developed an overlapping domain decomposition approach, called the bridging domain method, in which the energies of the atomistic and continuum models are scaled in the overlapping domain. Compatibility between the two models is enforced by Lagrange multipliers. A similar method was developed for molecular dynamics in Xiao and Belytschko [21]. A comparison of two types of coupling with bridging domain methods, L^2 and H^1 coupling, is given by Guidault and Belytschko [23]. Fish et al. [24] have developed a similar method in which the forces instead of the energies are scaled, which permits the continuum to be an irreversible material.

Wagner and Liu [14] developed a bridging scale method (BSM) for coupling molecular dynamics with continuum mechanics. In their method, the continuum and atomistic models are initially applied on the entire domain. Then the fine scale degrees of freedom are eliminated from the coarse scale domain by a time history kernel, i.e. a Green’s function. In the fine scale region a projection of the fine scale solution onto the coarse scale model is used to link the models. A Laplace transform was applied to derive the time history kernel function which corresponds to the missing degrees of freedom in the coarse scale region. Park et al. [37] extended the method to two dimensions by computing the kernel function numerically. The performance of BSM is studied by Farrell et al. [16].

In all concurrent coupling methods for dynamics, a general issue is the spurious reflection of elastic waves at the fine scale domain boundary due to the difference in the cutoff frequencies of the models. Several silent boundary conditions have been developed to solve this problem. Cai et al. [17] introduced a time-dependent memory kernel

to the equations of motion in the fine scale. It gave the exact boundary conditions for the microscale simulation but was generally computationally expensive. E and Huang [18] proposed a matching boundary condition by optimizing the reflection term which was added to the displacement field. This type of matching condition is only valid for zero temperature systems. The time history kernel of the bridging scale method [14] serves a similar purpose. In the bridging domain method [21], a diagonalized constraint matrix was used to eliminate such reflections. To and Li [19] applied a perfectly matched layer [20] to the overlapping region to absorb high frequency waves leaving the atomistic domain.

2 Classification of Methods

Before describing concurrent methods in more detail, we will first give an overview of different multiscale methods. Multiscale methods are often classified as either hierarchical or concurrent. But this classification is too simple to reflect the subtleties of different variants of multiscale analysis methods. Table 1 gives a classification of multiscale methods, and a schematic of the various methods is shown in Fig. 1.

In Fig. 1 the fine-scale models are on the left and the coarse scale model on the right. The essence of the procedures is the same for any scales that are linked, whether it is quantum to continuum, microstructure of a composite to an engineering structure, or an atomistic (molecular) model to a continuum. Furthermore, coarse-graining is not restricted to link only two scales: it is feasible to couple three, four or even more scales.

Tab. 1: Classification of multiscale methods illustrated for Atomistic/Continuum

Multiscale techniques	Information transfer
Hierarchical	$\Omega^{atomic} \rightarrow \Omega^{continuum}$
Hybrid hierarchical-semiconcurrent	$\Omega^{atomic} \rightarrow \Omega^{continuum}$ if $\mathbf{E} \in \mathcal{E}_I$ $\Omega^{atomic} \leftrightarrow \Omega^{continuum}$ if $\mathbf{E} \notin \mathcal{E}_I$
Semiconcurrent	$\Omega^{atomic} \leftrightarrow \Omega^{continuum}$
Concurrent	$\Omega^{atomic} \Leftrightarrow \Omega^{continuum}$

($\mathbf{E}$ =input, $\mathcal{E}_I$ =domain of input, $\rightarrow$, $\leftrightarrow$: weak coupling, $\Leftrightarrow$: strong coupling)

Hierarchical methods are the most widely used and computationally the most efficient, see Fig.1a. In these methods, the response of a representative volume element at the fine scale is first computed over a range of expected inputs $\mathcal{E}$, and from these a stress-strain law is extracted. The stress-strain law can be a constitutive equations, with parameters determined by the fine scale solutions, a numerical data base, or a neutral network based law. For linear response, this process can be simplified since there is a robust theory of homogenization whereby linear constants can be effectively extracted, sometimes even without recourse to numerical micromodels.

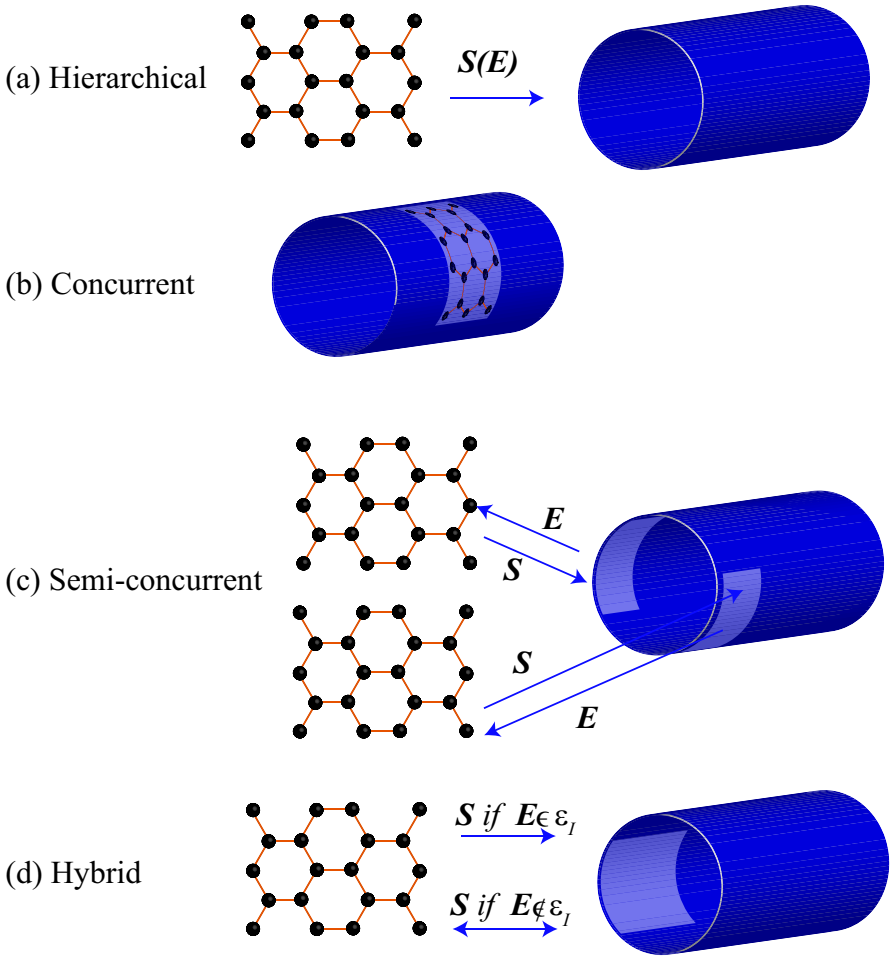

Fig. 1: Schematic of hierarchical, concurrent, semiconcurrent and hybrid hierarchical-semiconcurrent coupling methods.

For severely nonlinear problems, hierarchical models become more problematical, particularly if the fine scale response is path dependent. It should be noted that when failure occurs, in many circumstances hierarchical models are invalid and cannot be used, see Song et al. [15].

Concurrent methods are those in which the fine scale model is embedded in the coarse scale model and is directly and intimately coupled to it, as shown in Fig 1b. Both compatibility and momentum balance are enforced across the interface. For example, in Khare et al. [1, 2] electronic structure models solved by quantum mechanics (in the bond breaking subdomain) are linked to atomistic and continuum models. Similarly the MADD method [12], the BSM [14] and the bridging domain method [22] are concurrent. Such models are quite effective when the subdomain where a higher order theory is required is small compared to the domain of the problem. In Khare et al. [1, 2], the QM model, which is the highest order theory, was restricted to the area around a slit where bond breaking was likely to occur; some of these models are described in Section 5. In the study of fracture, fine scale models can be inserted in *hot spots* where stresses become large. These *hot spots* can be identified on the fly or by a previous run.

Semiconcurrent methods are a class of methods in which a fine scale model is calculated concurrently with a coarser-grained model, as shown in Fig. 1c. They are distinguished from concurrent methods by the fact that the fine scale model is not coupled directly with the coarse-grained model; compatibility and momentum balance are only satisfied approximately. Examples of such methods are the FE^2 methods of Feyel and Chaboche [28], and their extensions to gradient models in Kouznetsova et al. [29]. As discussed in [28], the reduction in computational effort from a fully concurrent approach is not great. The appeal of these methods lies more in the fact that the fine scale and coarse scale models can be run by separate software and the avoidance of numerical problems associated with rapid changes in element size (the lattice constant can be viewed as an element size). These difficulties include

- Ill-conditioning of the equilibrium equations
- Spurious reflections off the interface between fine-grain and coarse-grain models

The fourth type of methods are hybrid hierarchical/semiconcurrent methods, Fig.1d. In these methods, a hierarchical approach is used as long as the requested information is available. When the requested information is not available, i.e. when the strain is outside the strain domain $\mathcal{E}$ that has been exercised by the fine-scale model, a direct computation is then invoked. If the fine-scale response is history dependent, it would be necessary to reconstruct at least an approximate history.

3 Mechanical Equilibrium Methods

In this section we describe several concurrent methods for mechanical equilibrium problems, often called 0 K methods; we will often simply use the term equilibrium methods. In this description and subsequent descriptions of the method, we denote the complete domain in the initial configuration by Ω_0 and its boundaries by Γ_0; Γ_0 consists of traction boundaries Γ_0^t and the displacement boundaries Γ_0^u. The domain is subdivided into the subdomains treated by continuum mechanics (CM), Ω_0^C, by molecular mechanics (MM), i.e. by atomistic methods, Ω_0^M, and by quantum mechanics (QM), Ω_0^Q; $\Omega_0^M \cup \Omega_0^Q$ is the domain encompassed by the atoms of the model. The intersection of Ω_0^C and Ω_0^M is denoted by Ω_0^{MC} and is often called the handshake domain; Γ_0^α denotes the edges of the continuum domain. The position of atoms I in the reference configuration, or more precisely the nuclei of the atom I, is given by $\mathbf{X}_I$ and its displacements by $\mathbf{d}_I$. Sometimes we use a superscript A to indicate molecular mechanics related variables instead of M.

3.1 Direct and Master-Slave Coupling

A common method of coupling molecular mechanics with continuum mechanics is what we call master-slave coupling. It can also be used for QM/MM and QM/CM coupling. This is a well-known method in finite elements (see [5], p 168) based on energy. In one dimension, a model with direct coupling is illustrated in Fig. 2. As indicated by the dashed lines, the atoms and coincident nodes are constrained to move together. In master-slave coupling, the nodes need not be coincident. We will describe this more general coupling in more detail.

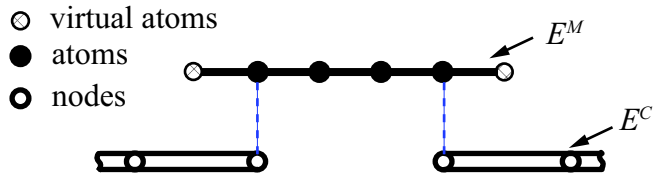

Fig. 2: Schematic of direct coupling method

The total energy of the coupled system is

$$E\left(\mathbf{u}, \mathbf{d}^M\right) = E^C\left(\mathbf{u}\right) + E^M\left(\mathbf{d}^M\right) - E^{\text{ext}} \tag{1}$$

where E^M and E^C are the energies of the molecular and continuum subdomains respectively, and E^{ext} is the work of external forces. The vector $\mathbf{u}$ is the displacement field in the continuum and $\mathbf{d}^M$ is a vector of discrete molecular displacements. The continuum energy is given by

$$E^C\left(\mathbf{u}\right) = \int_{\Omega_0^C} w_C\left(\mathbf{F}\right) d\Omega_0^C \tag{2}$$

where w_C is the strain energy density and $\mathbf{F}$ is the deformation gradient: $\mathbf{F} = \mathbf{I} + \frac{\partial \mathbf{u}}{\partial \mathbf{X}}$.

If a finite element method is used for the continuum, then the displacement field is given by

$$\mathbf{u}\left(\mathbf{X}\right) = \sum_{I \in \mathcal{S}} N_I\left(\mathbf{X}\right) \mathbf{u}_I \tag{3}$$

where $N_I(\mathbf{X})$ are the shape functions expressed as functions of the material coordinates $\mathbf{X}$, $\mathbf{u}_I$ are the nodal displacements and $\mathcal{S}$ is the set of all FEM nodes.

The potential energy of the bond $I-J$ is denoted by $w_{IJ}^M = w_M(\mathbf{x}_I, \mathbf{x}_J)$, where $\mathbf{x}_I = \mathbf{X}_I + \mathbf{d}_I$ is the current position of atom I. The total potential energy of the molecular mechanics subdomain Ω^M is then

$$E^M = \frac{1}{2}\sum_{I,J\in\mathcal{M}} w_{IJ}^M \tag{4}$$

where $\mathcal{M}$ is a set of atoms in the atomistic model.

Master-slave methods can be classified as follows:

- Methods with atoms coincident with continuum nodes on the interface, Fig. 3.
- Methods where atoms are not coincident with nodes on the interface, Fig 4.

An illustration of a model with coincident atoms/nodes is shown in Fig. 3. As can be seen, to reduce the nodal spacing to the lattice constant, it is necessary to construct rather complicated meshes. This is awkward in two dimensions and can be a severe obstacle in three dimensions.

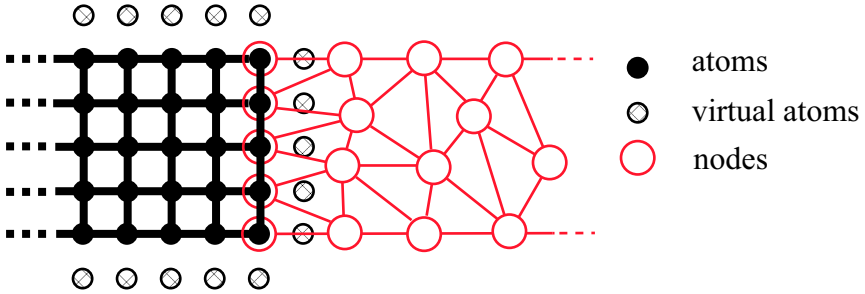

Fig. 3: Master-slave model with nuclei coincident with nodes at the coupling interface

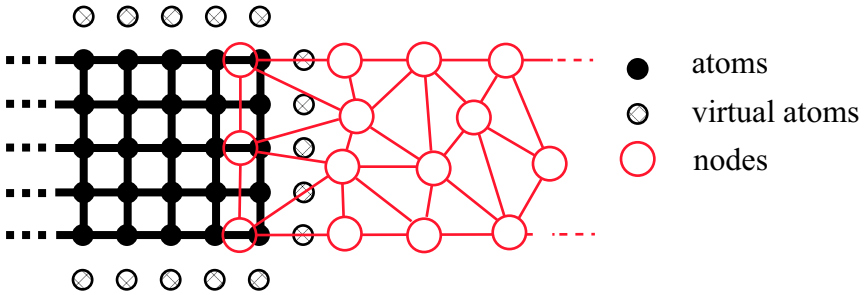

Fig. 4: Master-slave model with nuclei not coincident with nodes at the coupling interface

In models with coincident coupling, the atomistic and nodal displacements at the interface are taken to be equal. Therefore, we define a common vector $\mathbf{d} = \{\mathbf{d}_I\}_{I=1}^n$, where n is the number of independent nodes and atoms. Compatibility is enforced by letting

$$\mathbf{d}_I = \begin{cases} \mathbf{d}_I^M & \mathbf{X}_I \in \Omega_0^M \\ \mathbf{d}_I^M = \mathbf{u}_I & \mathbf{X}_I \in \Omega_0^M \cup \Omega_0^C \\ \mathbf{u}_I & \mathbf{X}_I \in \Omega_0^C \end{cases} \tag{5}$$

The discretized energy of the model can then be written as

$$E(\mathbf{d}) = E^C(\mathbf{d}) + E^M(\mathbf{d}) - E^{\text{ext}} \tag{6}$$

Equilibrium configurations correspond to the stationary points of (6), i.e the configurations where the derivatives with respect to $\mathbf{d}_I$ vanish. This gives

$$0 = \frac{\partial E^M}{\partial \mathbf{d}_I} + \frac{\partial E^C}{\partial \mathbf{d}_I} - \frac{\partial E^{\text{ext}}}{\partial \mathbf{d}_I} \tag{7}$$

These derivatives correspond to nodal and atomistic forces, so the above can be written as

$$0 = \mathbf{f}_I^M + \mathbf{f}_I^C - \mathbf{f}_I^{\text{ext}} \tag{8}$$

where from (2) and (3) it follows that

$$\mathbf{f}_I^C = \int_{\Omega_0^C} \frac{\partial w_C(\mathbf{F})}{\partial \mathbf{F}} \frac{\partial \mathbf{F}}{\partial \mathbf{d}_I} d\Omega_0^C = \int_{\Omega_0^C} \mathbf{P} \frac{\partial N_I}{\partial \mathbf{X}} d\Omega_0^C \tag{9}$$

where $\mathbf{P}$ is the first Piola-Kirchhoff stress.

The position of atoms which lie inside Ω_0^C, denoted as virtual atoms in Fig.3, are obtained by the finite element interpolation (3),

$$\mathbf{d}_J^M = \sum_{I \in \mathcal{S}} N_I(\mathbf{X}_J)\, \mathbf{u}_I \tag{10}$$

Models with noncoincident nodes and atoms at the interface, as shown in Fig.4, are treated by master-slave methods by letting the atoms be slaves. The displacement of the atoms on the interface are obtained by (10). The governing equations are identical to those described for coincident coupling. However, the forces on the slave atoms are added to the continuum nodes by the usual master-slave procedure. This can be seen by rederiving (6) for nodes on the interface:

$$\frac{\partial E^M}{\partial \mathbf{u}_I} = \sum_J \frac{\partial E^M}{\partial \mathbf{d}_J^M} \frac{\partial \mathbf{d}_J^M}{\partial \mathbf{u}_I} = \mathbf{f}_I^M N_J(\mathbf{X}_I) \tag{11}$$

where the last step follows from the definition of nodal forces and (10)

3.2 ONIOM Method

In the ONIOM method, first developed by Svensson et al. [32], the higher order method is superimposed on the lower order method on the subdomain in which higher accuracy is needed. For QM/MM coupling, the ONIOM method is basically a direct coupling method. The QM/CM coupling we describe is a master-slave method. Its advantage lies in the ease with which it can be used to couple models that reside in two different software systems. Since the QM and MM methods that are needed for a particular model are often in different software packages, this often proves useful. The ONIOM scheme is illustrated in one dimension in Fig. 5 for a quantum/molecular model. As can be seen, the model consists of three layers in the subdomain where the higher order theory is used:

- The layer Q modeled by the higher order theory, in this case an electronic structure method (quantum mechanics)
- The bottom layer M which extends throughout the entire computational domain, in this case an atomistic model
- The overlaid (middle) layer MQ which cancels the energy of the lower order method (molecular mechanics) on Ω^Q

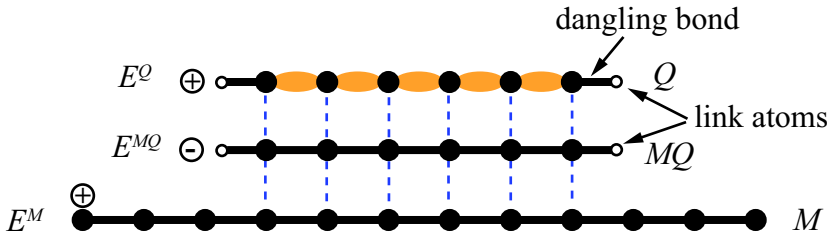

Fig. 5: Schematic of ONIOM method for quantum/molecular coupling. The signs indicate the sign of the corresponding terms in energy (force) expression; the vertical lines indicate that the atoms in the three models are constrained to move identically.

The middle layer is called fictitious, but both M and MQ are fictitious on Ω_Q. They are only retained to simplify the coupling.

In the ONIOM method, the displacements of corresponding nuclei in difference layers are equal (except the link atoms) and will here be denoted by $\mathbf{d}_I$.

The energy of the system as treated by ONIOM is given by

$$E\left(\boldsymbol{\alpha}\mathbf{d}\right) = E^Q\left(\boldsymbol{\alpha}\mathbf{d}\right) + E^M\left(\mathbf{d}\right) - E^{MQ}\left(\mathbf{d}\right) - E^{\text{ext}}\left(\mathbf{d}\right) \tag{12}$$

as is readily apparent from Fig. 5. Where $\mathbf{d}$ is the matrix of atomic displacements and $\boldsymbol{\alpha}$ the electronic configuration parameters. The equilibrium equations for a system with external loads $\mathbf{f}_I^{\text{ext}}$ on atom I is then

$$0 = \frac{\partial E}{\partial \mathbf{d}_I} = \frac{\partial E^Q}{\partial \mathbf{d}_I} + \frac{\partial E^M}{\partial \mathbf{d}_I} - \frac{\partial E^{MQ}}{\partial \mathbf{d}_I} - \mathbf{f}_I^{\text{ext}} \tag{13}$$

This equation can be written as

$$0 = \mathbf{f}_I^Q + \mathbf{f}_I^M - \mathbf{f}_I^{MQ} - \mathbf{f}_I^{\text{ext}} = \mathbf{f}_I^{\text{int}} - \mathbf{f}_I^{\text{ext}} \tag{14}$$

Generally, in the ONIOM coupling of QM/MM models, the atomic displacements $\mathbf{d}_I$ are obtained by minimizing the total energy with respect to the parameters of the electronic structure $\boldsymbol{\alpha}$ and $\mathbf{d}_I$. This involves two nested iterative procedures. First the energy must be minimized with respect to the parameters of the electronic structure. In the outer loop, the positions of the nuclei are updated to bring them towards equilibrium.

An interesting aspect of ONIOM is that the quality of the coarse scale model underlying the fragment has no effect on the results. Therefore, models that are quite inaccurate for the phenomena under study can be used. For example, in the study of fracture with MM/QM ONIOM schemes, the MM model can be quite inaccurate near the fracture strain. However, it is crucial that in the range of behavior that occurs at the QM/MM interface, the models are matched carefully. For example, in Khare et al. [1], it was reported that a standard Brenner MM model for carbon coupled with either a DFT or PM3 quantum model often fractured at the interface. Therefore, they proposed a scaling of the MM potential to provide better results. A major source of error in these models is the “dangling" bonds at the boundary of the model (in Fig. 5 the two ends of the model). Electronic structure calculations can be very inaccurate at nonperiodic boundaries when the QM model is terminated, especially for covalent bonds. One common remedy is to cap the dangling bonds with hydrogen atoms; these are called link atoms.

The ONIOM scheme can also be used for coupling an atomistic (molecular) or quantum model with a finite element model of a continuum. This procedure is schematically shown in Fig. 6 for a MM/CM model; the model consists of three layers

1. the low order model (in this case the continuum model)
2. a fictitious continuum model that overlays the fragment to be modeled by atomistics
3. the atomistic (molecular) model at the top in Fig. 6

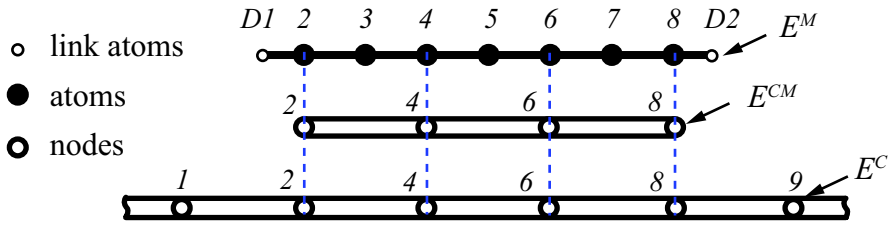

Fig. 6: ONIOM scheme for continuum (C)- molecular (M) coupling.

In this type of application, the nodal spacing of the continuum model need not coincide with the atomic spacing (lattice constant). Instead, the atomistic displacements can be computed by using the finite element interpolation. This is of advantage since the finite element continuum model need not be refined to the atomistic lattice at the coupling interface. Of course, if the disparity between the lattice constant and element size is too large, substantial error can be engendered.

The formulation framework is identical to that for QM/MM coupling by ONIOM. The energy of the continuum/atomistic system is

$$E\left(\mathbf{d}\right) = E^C\left(\mathbf{d}\right) + E^M\left(\mathbf{d}\right) - E^{CM}\left(\mathbf{d}\right) - E^{\text{ext}}\left(\mathbf{d}\right) \tag{15}$$

where the energies are associated with the models as shown in Fig. 6 and $\mathbf{d}$ is a vector of nodal displacements. For example, for the model in Fig. 6 $\mathbf{d}^T = [d_1, d_2, ..., d_9]$.

The equations of equilibrium are then

$$0 \quad = \quad \frac{\partial E}{\partial \mathbf{d}_I} = \frac{\partial E^C}{\partial \mathbf{d}_I} + \frac{\partial E^M}{\partial \mathbf{d}_I} - \frac{\partial E^{CM}}{\partial \mathbf{d}_I} - \mathbf{f}_I^{\text{ext}}$$

We note that as before, the derivatives with respect to the nodal displacements are nodal forces, so

$$0 = \quad \mathbf{f}_I^C + \mathbf{f}_I^M - \mathbf{f}_I^{CM} - \mathbf{f}_I^{\text{ext}} \tag{16}$$

As in QM/MM coupling, the major difficulty occurs on the edge of the atomistic domain, since the behavior of the outermost bonds (the far left and far right bonds in Fig. 5) can be polluted by incorrect placement of the link atoms D_1 and D_2.

3.3 Bridging Domain Method

In the following, we describe the bridging domain method for coupling continuum models with molecular models in mechanical equilibrium problems. The bridging domain method is in essence an overlapping domain decomposition scheme where compatibility in the overlapping (handshaking) domain is enforced by Lagrange Multipliers. The advantage of this method is that the atomic nuclei need not be coincident with the nodes of the continuum mesh. Furthermore, the method is generally used with a linear scaling of the energies in the handshaking domain, with the atomistic (continuum) energy dominant near the purely atomistic (continuum) domain. This enables the method to alleviate the error that arise from dropping atomistic energies due to far field atoms and provides a gradual transition from the molecular model to the continuum model. An example of a concurrent bridging domain model of graphene is shown in Fig. 7.

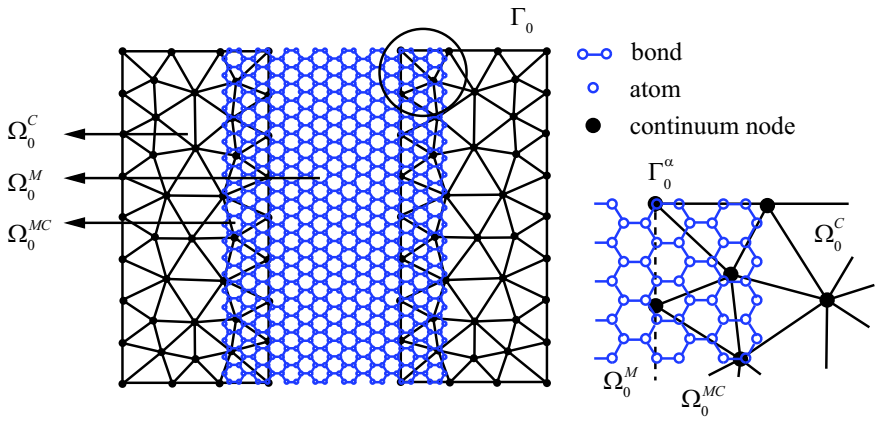

Fig. 7: Schematic of bridging domain method.

The total potential energy of the molecular mechanics subdomain Ω^M is given by (4) and the total potential energy of the continuum is given by (2). In expressing the total internal potential energy of the system, we employ a energy scaling function $\alpha(\mathbf{X})$ in the overlapping subdomain. The energy scaling function is defined as

$$\alpha(\mathbf{X}) = \begin{cases} 0 & \text{in } \Omega_0^M/\Omega^{MC} \\ l(\mathbf{X})/l_0(\mathbf{X}) & \text{in } \Omega_0^{MC} \\ 1 & \text{in } \Omega_0^C/\Omega_0^{MC} \end{cases} \tag{17}$$

where $l(\mathbf{X})$ is the least square projection of $\mathbf{X}$ onto Γ_0^α, as shown in Fig. 8, $l_0(\mathbf{X})$ is defined by the distance between the overlapping domain boundaries Γ_0^α on the orthogonal projection of $\mathbf{X}$. The scaling parameter vanishes at the edge of the continuum and is unity at the other edge of Ω_0^{MC}; Ω_0^{MC} should include the last line of atoms.

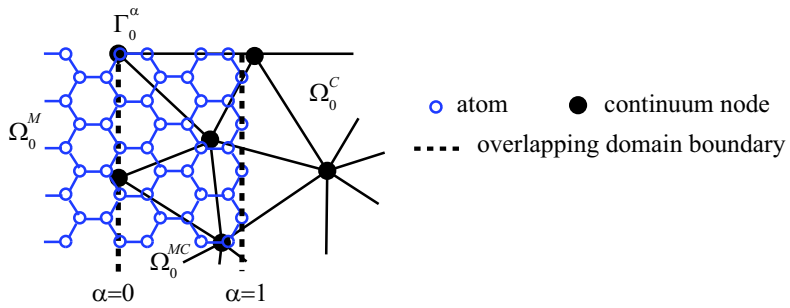

Fig. 8: Overlapping subdomain of atomistic and continuum model.

The total potential energy is given by

$$E_\alpha^C(\mathbf{u}) + E_\alpha^M(\mathbf{d}) = \int_{\Omega_0^C} \alpha(\mathbf{X})\, w_C(\mathbf{F}) d\Omega_0^C + \frac{1}{2} \sum_{I,J \in \mathcal{M}} (1 - \alpha_{IJ})\, w_{IJ}^M \tag{18}$$

where $\alpha_{IJ} = \frac{1}{2}(\alpha_I + \alpha_J)$, $\alpha_I = \alpha(\mathbf{X}_I)$, and $\mathbf{d}$ is the vector of atomic displacements. The external potential is scaled similarly, so

$$E_\alpha^{\text{ext}} = \int_{\Omega_0^C} \alpha\rho_0 \mathbf{b} \cdot \mathbf{u} d\Omega_0^C + \int_{\Gamma_0^t} \alpha\rho_0 \bar{\mathbf{t}} \cdot \mathbf{u} d\Gamma_0^t + \sum_{I \in \mathcal{M}} (1 - \alpha_I)\, \bar{\mathbf{f}}_I^{\text{ext}} \cdot \mathbf{d}_I \tag{19}$$

where $\bar{\mathbf{f}}_I^{\text{ext}}$ is any external force applied to atom I.

Let $\mathcal{M}^{MC} = \{I | \mathbf{X}_I \in \Omega_0^{MC}\}$ be the set of atoms initially in the handshaking region. In the initial version of the bridging domain method [22], displacement compatibility in the handshaking region Ω_0^{MC} was enforced by the constraint

$$g_I = ||\mathbf{u}(\mathbf{X}_I) - \mathbf{d}_I||^2 = \sum_{i=1}^{ND} [u_i(\mathbf{X}_I) - d_{iI}]^2 = 0 \,, \forall\, I \in \mathcal{M}^{MC} \tag{20}$$

where ND denotes number of dimensions. (20) requires that the continuum displacements conform to the atomic displacements at the discrete positions of the atoms. Later versions of the bridging domain method [21, 30] have used the following stronger constraint

$$g_{iI} = u_i(\mathbf{X}_I) - d_{iI} = 0 \,, \forall\, I \in \mathcal{M}^{MC} \;\&\; i = 1..ND \tag{21}$$

We note that by (20) a single constraint is applied per atom in $\mathcal{M}^{MC}$ whereas by (21) one constraint is applied for each component of the displacement of each atom. The use of constraint (20) rather than (21) results in a system of equation with fewer Lagrange multipliers but it quite peculiar and not recommended. For this reason (21) will be used in the following derivation.

We first show how the constraint is applied by the Lagrange multiplier method; then we will add the modifications needed for the augmented Lagrangian method.

In the Lagrange multiplier method, the problem is posed as follows: find the stationary point of

$$W_L = E_\alpha^C + E_\alpha^M - E_\alpha^{\text{ext}} + \boldsymbol{\lambda}^T \mathbf{g} \tag{22}$$

where $\boldsymbol{\lambda} = \{\lambda_{iI}\}$ is the vector of Lagrange multipliers and $\boldsymbol{g} = \{g_{iI}\}$ is a vector of constraints. The Lagrange multiplier λ_{iI} is the generalized force that enforces the constrain g_{iI} given by (21).

To develop the corresponding discrete equations, we use a finite element method (FEM) in Ω_0^C and molecular mechanics in Ω_0^M. The displacements in Ω_0^C are given by (3). The Lagrange multiplier field is expressed in terms of shape functions denoted by $N^\lambda(\mathbf{X})$:

$$\boldsymbol{\lambda}(\mathbf{X}, t) = \sum_{I \in \mathcal{S}^\lambda} N_I^\lambda(\mathbf{X})\, \bar{\boldsymbol{\lambda}}_I(t) \tag{23}$$

where $\mathcal{S}^\lambda$ is the set of all nodes of the Lagrange multiplier mesh. Generally, the shape functions for the Lagrange multiplier field will differ from those for the displacements, $N_I(\mathbf{X})$, and they must satisfy the LBB conditions. The Lagrange multiplier field is usually constructed by an auxiliary finite element triangulation of the intersection (overlapping) domain, as shown in Fig. 9. To distinguish the Lagrange multiplier $\boldsymbol{\lambda}_I$ in (22) from the nodal values at the field, we use $\bar{\boldsymbol{\lambda}}_I$ to denote the Lagrange multipliers at the Lagrange multiplier nodes.

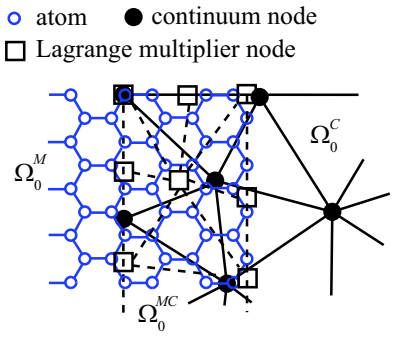

Fig. 9: Lagrange multiplier interpolation in the overlapping region.

The discrete equilibrium equations are then obtained substituting (3-23) into W_L (22) and setting the derivatives of W_L with respect to $\mathbf{u}_I$, $\mathbf{d}_I$ and $\bar{\boldsymbol{\lambda}}_I$ to zero, which yields the following equations

$$\frac{\partial W_L}{\partial u_{iI}} = \left(F_{iI}^{\text{int}} - F_{iI}^{\text{ext}}\right) + \sum_{J \in \mathcal{M}^{MC}} \lambda_{iJ} N_{IJ} = 0, \; \forall I \in \mathcal{S} \tag{24}$$

$$\frac{\partial W_L}{\partial d_{iI}} = \left(f_{iI}^{\text{int}} - f_{iI}^{\text{ext}}\right) - \lambda_{iI} = 0,\ \forall I \in \mathcal{M} \tag{25}$$

$$\frac{\partial W_L}{\partial \bar{\lambda}_{iI}} = \sum_{J \in \mathcal{M}^{MC}} N_{IJ}^{\lambda} g_{iJ} = 0,\ \forall I \in \mathcal{S}^{\lambda} \tag{26}$$

where $N_{IJ} = N_I\left(\mathbf{X}_J\right)$, $N_{IJ}^{\lambda} = N_I^{\lambda}\left(\mathbf{X}_J\right)$, $\lambda_{iI} = \lambda_i\left(\mathbf{X}_I\right)$ and

$$F_{iI}^{\text{int}} = \int_{\Omega_0^C} \alpha \frac{\partial w_C\left(\mathbf{F}\right)}{\partial u_{iI}} d\Omega_0^C \tag{27}$$

$$f_{iI}^{\text{int}} = \frac{1}{2} \sum_{I,J \in \mathcal{M}} \left(1 - \alpha_{IJ}\right) \frac{\partial w_{IJ}^M}{\partial d_{iI}} \tag{28}$$

$$F_{iI}^{\text{ext}} = \frac{\partial E^{\text{ext}}}{\partial u_{iI}} \tag{29}$$

$$f_{iI}^{\text{ext}} = \frac{\partial E^{\text{ext}}}{\partial d_{iI}} \tag{30}$$

The augmented Lagrangian method can be developed by adding a penalty to (22) as follows:

$$W_{AL} = E_{\alpha}^C + E_{\alpha}^M - E_{\alpha}^{\text{ext}} + \boldsymbol{\lambda}^T \mathbf{g} + \frac{1}{2} p \mathbf{g}^T \mathbf{g} \tag{31}$$

where p is the penalty parameter; if $p = 0$, (31) is identical to (22).

The discrete equations for the augment Lagrangian method form of the bridging domain method are obtained by inserting (3) and (23) into (31) and setting the derivatives of W_{AL} with respect to $\mathbf{u}_I$, $\mathbf{d}_I$ and $\bar{\boldsymbol{\lambda}}_I$ to zero. This gives

$$\frac{\partial W_{AL}}{\partial u_{iI}} = \frac{\partial W_L}{\partial u_{iI}} + p \sum_{J \in \mathcal{M}^{MC}} g_{iJ} N_{IJ} = 0,\ \forall I \in \mathcal{S} \tag{32}$$

$$\frac{\partial W_{AL}}{\partial d_{iI}} = \frac{\partial W_L}{\partial d_{iI}} - p\, g_{iI} = 0,\ \forall I \in \mathcal{S} \tag{33}$$

$$\frac{\partial W_{AL}}{\partial \bar{\lambda}_{iI}} = \frac{\partial W_L}{\partial \bar{\lambda}_{iI}} = 0,\ \forall I \in \mathcal{S}^{\lambda} \tag{34}$$

We have found that in general, the bridging domain method works best when the Lagrange multiplier fields are Dirac delta functions at the locations of the nuclei. This choice of Lagrange multipliers enforces compatibility exactly with the finite element approximation for the continuum. We can write this approximation for the Lagrange multipliers as

$$\boldsymbol{\lambda}\left(\mathbf{X}\right) = \sum_{I \in \mathcal{M}^{MC}} \hat{\boldsymbol{\lambda}}_I \delta\left(\mathbf{X} - \mathbf{X}_I\right) \tag{35}$$

where $\hat{\boldsymbol{\lambda}}_I$ are the unknown values of the Lagrange multipliers and $\delta(\bullet)$ is the Dirac delta function. For the strict Lagrange multiplier method, the discrete equations are

$$\frac{\partial W_{AL}}{\partial u_{iI}} = \left(F_{iI}^{\text{int}} - F_{iI}^{\text{ext}}\right) + \sum_{J \in \mathcal{M}^{MC}} \hat{\lambda}_{iJ} N_{IJ} + p \sum_{J \in \mathcal{M}^{MC}} g_{iJ} N_{IJ} = 0,\ \forall I \in \mathcal{S} \tag{36}$$

$$\frac{\partial W_{AL}}{\partial d_{iI}} = \left(f_{iI}^{\text{int}} - f_{iI}^{\text{ext}}\right) - \hat{\lambda}_{iI} - p\, g_{iI} = 0,\ \forall I \in \mathcal{M} \tag{37}$$

$$\frac{\partial W_{AL}}{\partial \hat{\lambda}_{iI}} = g_{iI} = 0,\ \forall I \in \mathcal{S}^{\lambda} \tag{38}$$

Ghost Forces. In an ideal coupling scheme the forces acting on the atoms in the handshaking domain should be exactly those that would occur if the whole domain were modeled by atomistics. The difference between the ideal

forces acting of the atoms and the actual multiscale model forces are termed *ghost forces*. In many multiscale methods the ghost forces occur, even for linear homogeneous deformations and harmonic atomistic potentials - a study of the solutions to this problem for the various quasicontinuum methods can be found in Curtin and Miller [31].

In this subsection will we address the issue of ghost forces in the bridging domain method. We will show that for a linear elastic continuum and a molecular model with nearest neighbor interaction and a harmonic potential, ghost forces are eliminated when the pointwise Lagrange multiplier approximation (35), which we will also call strict coupling, is used; however, when the Lagrange multipliers are interpolated by finite element shape functions as in (23) ghost forces exist.

Consider the one-dimensional lattice depicted in Fig.10a with a harmonic potential with constant k. This is equivalent to a linear elastic constitutive model for the continuum with the elastic modulus $Y = a\mathsf{k}$, where a is the lattice constant. For this simple molecular system a consistent multiscale method (i.e. one without ghost forces) should satisfy the patch test, i.e. be able to reproduce a constant strain field exactly.

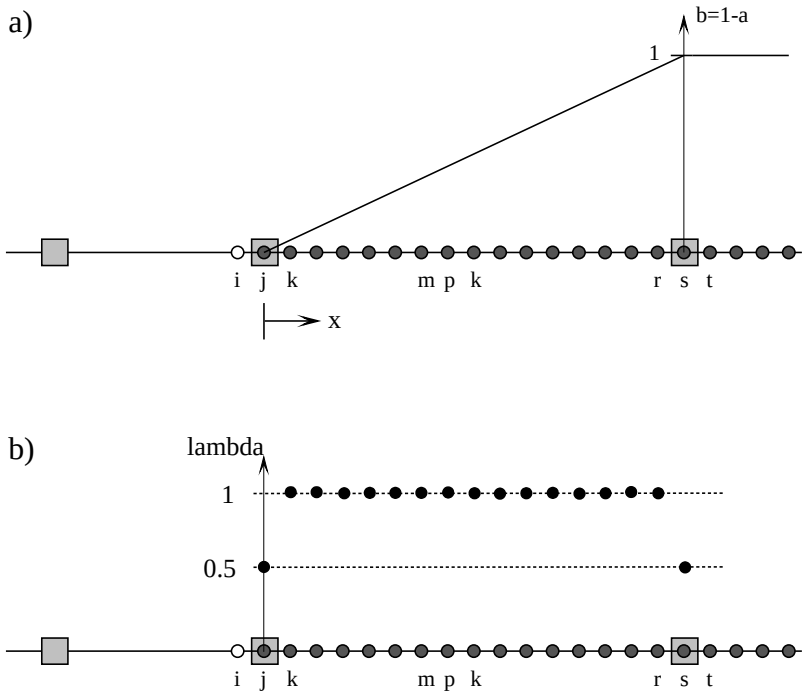

Fig. 10: Illustration of the bridging domain in one-dimension. Red circles represent atoms and grey squares represent FEM nodes

Let $\beta_i = \beta(X_i) = 1 - \alpha(X_i)$ and $\beta_{ij} = (\beta_i + \beta_j)/2$. For the coupled model shown in Fig.10a, the weight function β has a value of unity at atom s and decreases linearly to zero at atom j. The coupling domain spans only one element and so the energy scaling function is given by

$$\beta(\bar{x}) = \frac{\bar{x}}{h_e} = \frac{\bar{x}}{a\,(n-1)} \tag{39}$$

where h_e is the element length, a is the lattice spacing, n is the number of atoms in the handshaking domain. Note that both atoms j and s are assumed to be in the coupling domain.

Consider the uniform straining of the lattice in Fig.10a, such that each atomistic bond is elongated by Δ. For simplicity we will only study the Lagrange multiplier method with $p = 0$. The equilibrium equations, given by (26) or (38), for atoms j, p and s are respectively given by

$$r_j = \mathsf{k}\Delta\,(\beta_{ij} - \beta_{jk}) + \lambda\,(\mathbf{X}_i) = -\mathsf{k}\Delta\beta_{ij} + \lambda\,(\mathbf{X}_i) \tag{40}$$

$$r_p = \mathsf{k}\Delta\,(\beta_{mp} - \beta_{pq}) + \lambda\,(\mathbf{X}_p) \tag{41}$$

$$r_s \quad = \quad \mathsf{k}\Delta\left(\beta_{rs} - \beta_{st}\right) + \lambda\left(\mathbf{X}_s\right) = \mathsf{k}\Delta\left(\beta_{rs} - 1\right) + \lambda\left(\mathbf{X}_s\right) \tag{42}$$

where r_i is the residual force on atom i and is equal to the ghost force of atom i. For the bridging domain method to satisfy the patch test, the residual at all atoms must be zero, which gives

$$\lambda\left(\mathbf{X}_j\right) \quad = \quad \frac{1}{2}\frac{\mathsf{k}\Delta}{(n-1)}\lambda\left(\mathbf{X}_p\right) = \frac{\mathsf{k}\Delta}{(n-1)} \tag{43}$$

$$\lambda\left(\mathbf{X}_s\right) \quad = \quad \frac{1}{2}\frac{\mathsf{k}\Delta}{(n-1)} \tag{44}$$

The discrete Lagrange multipliers required to satisfy the patch test are shown in Fig.10b. We can see from this figure and equations (43-44) that in general a linear Lagrange multiplier field cannot provide the Lagrange multipliers needed to satisfy the patch test. Therefore, ghost forces will always exist in the bridging domain method when the Lagrange multipliers are interpolated by shape functions as in (23); however, when strict Lagrange multipliers (35) are used no ghost forces occur.

The conclusions of the previous paragraph are verified numerically in the following example. Consider a one-dimensional domain of length 128, with the origin of the coordinate system located at the left end. The atomistic subdomain is $0 \leq x \leq 80$ and the continuum subdomain is $64 \leq x \leq 128$, so the handshaking domain is $64 \leq x \leq 80$. The lattice spacing is taken to be $a = 1$ and a uniform finite element mesh is used with the element size is selected so that the handshaking domain is spanned exactly by a single element, so $h_e = 16a$. The atom at $x = 0$ is fixed and a displacement of magnitude 1 is applied to the node at $x = 128$.

In Fig. 11 the value of the Lagrange multipliers at each atom in the handshaking domain are shown for the bridging domain method with weak coupling (23) and strict coupling (35). The values are normalized by $\frac{\mathsf{k}\Delta}{(n-1)}$. The normalized L^2 error norm in the displacements given by

$$\text{Normalized } L^2 \text{ error norm} = \frac{1}{n^A}\sqrt{\sum_{I=1}^{n^A}\frac{\left(d_I - u^{\text{exact}}(X_I)\right)^2}{\left(u^{\text{exact}}(X_I)\right)^2}} \tag{45}$$

For strict coupling the error is zero to within machine precision and therefore the strict coupling method passes the patch test. We can observe that the Lagrange multipliers required to satisfy the patch test, as shown in 11, are those given by equations (43-44). The normalized L^2 error norm is 1.9×10^{-4} for the bridging domain method with weak coupling (23) and so it does not pass the patch test. This is because a linear field cannot exactly interpolate the required Lagrange multipliers given by (43-44). We note that although the bridging domain method with weak coupling does not exactly satisfy the patch test, the error in the solution is small.

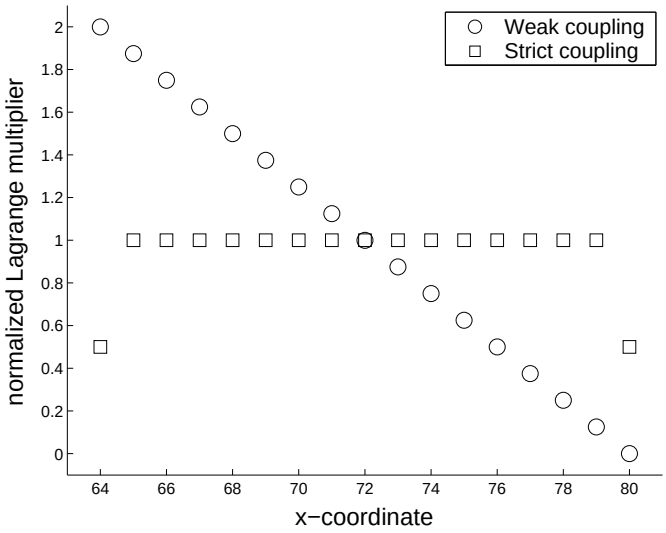

Fig. 11: Lagrange multipliers solution from the bridging domain method for a patch test on a one-dimensional lattice.

Stability of Lagrange Multiplier Methods. The development of molecular/continuum methods parallels recent work in the finite element community on the *gluing* of disjoint meshes in an overlapping subdomain. Ben Dhia and Rateau [26, 27] were the first to study these methods and developed a new method which is discussed below. They called these methods Arlequin methods. They showed that for a constant scaling in the overlapping domain, such as in the original handshake methods of Abraham et al. [12], instabilities appear in the Lagrange multiplier problem. In [27], a comparison of two coupling methods was made. To be more specific, in terms of an atomistic/continuum coupling, the energy of the coupled model is given by

$$E = E^A(\alpha) + E^C(\alpha) + (\boldsymbol{\lambda}, \delta\mathbf{u}) \tag{46}$$

where E is the total energy, $E^A(\alpha)$ in the scaled atomistic energy, $E^C(\alpha)$ in the scaled continuum energy and $(\lambda, \delta u)$ is a scalar product of the Lagrange multiplier field λ and the difference in displacements, as in the bridging domain method [22, 21]. The two types of coupling studied by Ben Dhia were called L^2 and H^1 couplings in [27] and are given respectively by

$$(\boldsymbol{\lambda}, \delta\mathbf{u}) = (\boldsymbol{\lambda}, \delta\mathbf{u})_{\mathcal{L}^2(\Omega_B)} = \int_{\Omega_B} \boldsymbol{\lambda} \cdot \delta\mathbf{u} d\Omega \equiv \int_{\Omega_B} \lambda_i \delta u_i d\Omega \tag{47}$$

$$\begin{aligned}(\boldsymbol{\lambda}, \delta\mathbf{u}) &= (\boldsymbol{\lambda}\delta\mathbf{u})_{\mathcal{H}^1(\Omega_B)} = \int_{\Omega_B} \left(\boldsymbol{\lambda} \cdot \delta\mathbf{u} + l^2 \epsilon(\boldsymbol{\lambda}) : \epsilon(\delta\mathbf{u})\right) d\Omega \\ &\equiv \int_{\Omega_B} \left(\lambda_i \delta u_i + l^2 \lambda_{i,j} \delta u_{i,j}\right) d\Omega \end{aligned} \tag{48}$$

It was shown in [27] that for the linear scaling of the energy, the L^2 coupling used in the bridging domain method is also stable. These conclusions also apply to atomistic/continuum coupling.

3.4 Quasicontinuum Method

The quasicontinuum method, as presented in Tadmor et al. [8], is a landmark work in atomistic/continuum coupling. It was one of the first works to introduce the concept of using Cauchy-Born rule in the continuum part of the model, so that the two models are compatible. Many of the difficulties in atomistic/continuum coupling, such as internal modes, are also dealt with in the subsequent papers.

From coupling point of view, the quasicontinuum method [8] is basically a direct atomistic-continuum coupling scheme where real atoms are coincident with the finite element nodes. Therefore, as in any direct coupling method, the mesh size must be decreased to the atomistic lattice spacing wherever atomistic potentials are to be used, which complicates mesh generation. For example, for a problem with several interacting dislocation in three dimensions, meshing could be quite difficult.

The pioneering contribution of the method is the seamless way it transitions from an atomistic description to a continuum description based of the Cauchy-Born rule. Because of this uniformity of the underlying material model, no abnormalities are introduced by differences in the material models at each scales. This concept has been widely adopted in other concurrent atomistic/continuum methods such as the bridging domain method.

It is also of interest that the quasicontinuum method avoids ill-posedness of the continuum model, i.e. in areas of bond breaking, for in these areas the method transitions to atomistic potentials, which are called nonlocal models. This process introduces a length scale wherever there is bond breaking. Thus, although an instable process is modeled, the system remain well posed.

4 Molecular Dynamics Systems

Most of the methods for coupling atomistic to continua are also applicable to dynamics. The major difficulty that arises in extending these methods to dynamics is that when the cutoff frequency of the continuum model is below that of the molecular dynamics model, spurious reflections occurs at the interface. This relationship of cutoff frequencies is almost always the case, since there is no benefit in using continuum model unless the internodal spacing is greater than the lattice constant. The cutoff frequency of a continuum model with low order elements is given by

$$\omega_{max}^{C} = \frac{c}{h_{min}} \tag{49}$$

where c is the wavespeed and h_{min} is the smallest distance between nodes. It can be shown with the Cauchy-Born rule that the atomistic cutoff frequency is of a crystal lattice

$$\omega_{max}^{A} = \frac{c}{l} \tag{50}$$

where c is the group wave velocity (an atomic lattice is dispersive) and l is the lattice constant. It is clear from the above that phonons in the atomistic domain with frequencies above ω_{max}^{C} will not be able to penetrate into the continuum model. This results in spurious reflections of high frequency phonons, which needs to be mitigated. The phonons above the atomic cutoff frequency represent thermodynamic energy that is not represented in the continuum model. It can be treated by linking the energy equation to a thermostat. One such approach is discussed in [21].

We next consider the concurrent coupling of molecular dynamics with continuum mechanics by the bridging domain method. For simplicity, we consider only pair potentials. The Hamiltonians of the atomistic and continuum subdomains are

$$H_M = \frac{1}{2} \sum_{I,J \in \mathcal{M}} w_{IJ}^{M} + \frac{1}{2} \sum_{I \in \mathcal{M}} M_I^M \dot{d}_{iI} \dot{d}_{iI} \tag{51}$$

$$H_C = \int_{\Omega_0^C} w_C(\mathbf{F}) d\Omega_0^C + \frac{1}{2} \sum_{I \in \mathcal{S}} M_I^C \dot{u}_{iI} \dot{u}_{iI} \tag{52}$$

where M^M denotes the mass of atoms and M^C the mass of nodes in the lumped mass matrix. Indicial notation convention applies to lower case indices, so repeated indices indicate summation.

To derive the equations of motion, it is convenient to transform Hamiltonian to the corresponding Lagrangian L. The same energy scaling function as for equilibrium systems (17) is used in the bridging domain. Lagrange multipliers are used to enforce the constraints between the atoms and the continuum mesh. In this case, the pointwise Lagrange multiplier field is used, so

$$\begin{aligned} L &= \frac{1}{2} \sum_{I \in \mathcal{M}} (1 - \alpha_I) M_I^M \dot{d}_{iI} \dot{d}_{iI} - \sum_{I \in \mathcal{M}} \sum_{J \in \mathcal{M} > I} w_{IJ}^{M} (1 - \alpha_{IJ}) \\ &+ \frac{1}{2} \sum_{I \in \mathcal{S}} \alpha_I M_I^C \dot{u}_{iI} \dot{u}_{iI} - \int_{\Omega_0^C} \alpha w_C d\Omega_0^C + G \end{aligned} \tag{53}$$

where

$$G = \sum_{J \in \mathcal{M}} \lambda_{iJ} \left(\sum_{I \in \mathcal{S}} N_{IJ} u_{iI} - d_{iJ} \right) \tag{54}$$

After this transformation, the equations of motion can be obtained by using Lagrange's equation

$$\frac{d}{dt} \left(\frac{\partial L}{\partial \dot{q}_i} \right) - \frac{\partial L}{\partial q_i} = 0 \tag{55}$$

where $\mathbf{q} = [\{d_{iI}\}, \{u_{iI}\}, \{\lambda_{iI}\}]$. This yields

$$\bar{M}_I^M \ddot{d}_{iI} + f_{iI}^{\text{int}} + \bar{f}_{iI}^{GM} = 0 \qquad i = 1 \ldots n_{SD} \tag{56}$$

$$\bar{M}_I^C \ddot{u}_{iI} + F_{iI}^{\text{int}} + \bar{f}_{iI}^{GM} = 0 \qquad i = 1 \ldots n_{SD} \tag{57}$$

$$\sum_{J \in \mathcal{S}} N_{JI} u_{iJ} - d_{iI} = 0 \qquad i = 1 \ldots n_{SD} \tag{58}$$

where $\bar{M}_I^C$ is a diagonalized mass matrix.

$$\bar{M}_I^M = (1-\alpha_I)\, M_I^M \tag{59}$$
$$\bar{M}_I^C = \sum_{J\in\mathcal{S}} \int_{\Omega_0^C} \alpha\rho_0 N_I N_J d\Omega_0^C \tag{60}$$
$$\tag{61}$$

The equations are integrated by a predictor-corrector central difference method (which is equivalent to the Verlet method) for time integration. The acceleration at time step n can be expressed as

$$\ddot{d}^n = \frac{d^{n+1} - 2d^n + d^{n-1}}{\Delta t^2} \tag{62}$$
$$\ddot{u}^n = \frac{u^{n+1} - 2u^n + u^{n-1}}{\Delta t^2} \tag{63}$$

Substituting (62) and (63) into (56) and (57), respectively, we get the displacements at step $n+1$

$$d_{iI}^{n+1} = -\frac{f_{iI}^{int}}{\bar{M}_I^M} + 2d_{iI}^n - d_{iI}^{n-1} + \frac{\Delta t^2 \sum_{J\in\mathcal{M}} \lambda_{iJ}^n \delta_{IJ}}{\bar{M}_I^M} \tag{64}$$
$$u_{iI}^{n+1} = -\frac{F_{iI}^{int}}{\bar{M}_I^M} + 2u_{iI}^n - u_{iI}^{n-1} - \frac{\Delta t^2 \sum_{J\in\mathcal{M}} \lambda_{iJ}^n N_{IJ}}{\bar{M}_I^C} \tag{65}$$

The equations for the Lagrange multipliers can be obtained by substituting the above displacements into the constraint (58)

$$\sum_{L\in\mathcal{M}} \lambda_{iL}^n A_{IL} = -\frac{f_{iI}^{int}}{\bar{M}_I^M} + \frac{2d_{iI}^n - d_{iI}^{n-1}}{\Delta t^2} + \sum_{J\in\mathcal{S}} N_{JI} \left(\frac{F_{iJ}^{int}}{\bar{M}_J^C} - \frac{2u_{iJ}^n - u_{iJ}^{n-1}}{\Delta t^2} \right) \tag{66}$$

where

$$A_{IL} = -\sum_{J\in\mathcal{S}} \frac{N_{JI} N_{JL}}{\bar{M}_J^C} - \frac{\delta_{IL}}{\bar{M}_I^M} \tag{67}$$

is called the consistent constraint matrix. These Lagrange multipliers are then used in (56) and (57) for a corrector calculation because that is essential for suppressing spurious reflections so a diagonalized constraint matrix $\mathbf{B}$ is used in the implementation

$$B_{IJ} = \begin{cases} 0 & I \neq J \\ \sum_{L\in\mathcal{M}} A_{IL} & I = J \end{cases} \tag{68}$$

This is discussed further in Section 5.

4.1 Conservation Properties of Bridging Domain Method

In the following we show the conservation of both linear momentum and the energy of the system in the bridging domain method. The conservation of angular momentum is shown in [33]. The work of Hairer et al. [34] shows that for the central difference method (symplectic Verlet), the energy is conserved in time if the ordinary differential equations in time are conservative. Therefore we only examine the time derivatives of the conservation variables.

The analysis shows that the bridging domain method exactly conserves linear momentum and energy. This presents the dilemma: how can the method suppress spurious reflections? As will be shown with numerical results, the answer lies in the diagonalization, which renders the method to be dissipative and remarkably effective in suppressing spurious reflections.

Conservation of Linear Momentum. The system linear momentum p_i is

$$p_i = p_i^M + p_i^C = \sum_{I\in\mathcal{M}} \bar{M}_I^M \dot{d}_{iI} + \sum_{J\in\mathcal{S}} \bar{M}_J^C \dot{u}_{iJ} \tag{69}$$

where $\bar{M}_I^M$ and $\bar{M}_I^C$ are defined in (59) and (60), respectively. The rate of change of the total linear momentum of the discrete system is given by

$$\frac{dp_i}{dt} = \frac{d}{dt}\left(\sum_{I\in\mathcal{M}} \bar{M}_I^M \dot{d}_{iI} + \sum_{J\in\mathcal{S}} \bar{M}_J^C \dot{u}_{iJ}\right) \tag{70}$$

Substituting Eq. (56-61) into Eq. (70)

$$\begin{aligned}\frac{dp_i}{dt} &= \sum_{I\in\mathcal{M}} \lambda_{iI} - \sum_{I,J\in\mathcal{M}} \frac{\partial w_{IJ}^M}{\partial d_{iI}}\alpha_{IJ} - \sum_{I\in\mathcal{M}} \lambda_{iI} \sum_{J\in\mathcal{S}} N_{JI} \\ &- \sum_{I\in\mathcal{S}} \int_{\Omega_0^C} (1-\alpha)\frac{\partial N_I}{\partial X_j} P_{ji} d\Omega_0^C \end{aligned} \tag{71}$$

By the partition of unity property of finite element interpolants, $\sum_{J\in\mathcal{S}} N_J(\mathbf{X}) = 1$ for $\forall \mathbf{X}$, thus the first and the third terms cancel. The fourth term vanishes, which can easily be seen if the summation is pulled into the integral and the partition-of-unity property of the shape functions is invoked. This partition of unity property has also been used to show the conservation properties of meshfree methods in Belytschko et al.[35]. The second term vanishes because of its antisymmetry on I and J, for example, w_{IJ}^M is a function of $||\mathbf{x}_I - \mathbf{x}_J||$ for a two body potential, so

$$\sum_{I,J\in\mathcal{M}} \frac{\partial w_{IJ}^M}{\partial d_{iI}} = \frac{1}{2}\sum_{I,J\in\mathcal{M}} \left(\frac{\partial w_{IJ}^M}{\partial d_{iI}} + \frac{\partial w_{IJ}^M}{\partial d_{iJ}}\right) = 0 \tag{72}$$

It can be shown that this term also vanishes for other potentials, such as the angle bending potential. So $dp_i/dt = 0$, which shows that linear momentum is conserved. The conservation property is independent of the form of the scaling function in the coupling domain.

Conservation of Energy. The time derivative of the total energy reads

$$\dot{E}^{tot} = \dot{T}^M + \dot{W}^M + \dot{T}^C + \dot{W}^C \tag{73}$$

where

$$\dot{T}^M = \sum_{I\in\mathcal{M}} \bar{M}_I^M \ddot{d}_{iI}\dot{d}_{iI} \tag{74}$$

$$\dot{W}^M = \sum_{I\in\mathcal{M}} \sum_{J\in\mathcal{M}>I} \left(\frac{\partial w_{IJ}^M}{\partial d_{iI}}\dot{d}_{iI} + \frac{\partial w_{IJ}^M}{\partial d_{iJ}}\dot{d}_{iJ}\right)(1-\alpha_{IJ}) \tag{75}$$

$$\dot{T}^C = \sum_{I\in\mathcal{S}} \bar{M}_I^C \ddot{u}_{iI}\dot{u}_{iI} \tag{76}$$

$$\dot{W}^C = \int_{\Omega_0^C} \alpha \frac{\partial w_C}{\partial \mathbf{F}} : \dot{\mathbf{F}} d\Omega_0^C = \int_{\Omega_0^C} \alpha \mathbf{P} : \dot{\mathbf{F}} d\Omega_0^C \tag{77}$$

Substituting (56-57) into (74-77)

$$\begin{aligned}\dot{E}^{tot} &= -\sum_{I\in\mathcal{M}} (\bar{f}_{iI}^{int} + \frac{\partial G}{\partial d_{iI}})\dot{d}_{iI} - \sum_{I\in\mathcal{S}} (\bar{F}_{iI}^{int} + \frac{\partial G}{\partial u_{iI}})\dot{u}_{iI} \\ &- \sum_{I\in\mathcal{M}} \sum_{J\in\mathcal{M}>I} \left(\frac{\partial w_{IJ}^M}{\partial d_{iI}}\dot{d}_{iI} + \frac{\partial w_{IJ}^M}{\partial d_{iJ}}\dot{d}_{iJ}\right)(1-\alpha_{IJ}) + \int_{\Omega_0^C} \alpha \mathbf{P} : \frac{\partial N_I}{\partial \mathbf{X}} d\Omega_0^C \dot{u}_{iI} \\ &= \sum_{I\in\mathcal{M}} \frac{\partial G}{\partial d_{iI}}\dot{d}_{iI} - \sum_{I\in\mathcal{S}} \frac{\partial G}{\partial u_{iI}}\dot{u}_{iI} = -\dot{G} \end{aligned} \tag{78}$$

Since G is the constraint term which vanishes by the Karush-Kuhn-Tucker condition, the energy is conserved.

4.2 Master-Slave and Handshake Methods

The master-slave method can be applied to MM/CM coupling by either edge-to-edge to overlaid domain decomposition. In either case, the position of any atom which is common to the continuum and atomistic domains is given by

$$\mathbf{d}_J = \sum N_I\left(\mathbf{X}_J\right)\mathbf{u}_I \quad \text{or} \quad \mathbf{d} = \mathbf{N}\mathbf{u}^C \tag{79}$$

The nodal forces and mass of the atoms are distributed to the nodes of the continuum elements or edges that are overlaid by the atoms. Using standard master slaving coupling formulas based on energy (see [5]), these additional forces and masses

$$\mathbf{f}_I = \sum_J \mathbf{N}_I\left(\mathbf{X}_J\right)\mathbf{f}_J^M \quad \text{or} \quad \mathbf{f} = \mathbf{N}^T\mathbf{f}^M \tag{80}$$

$$\mathbf{M}_{IJ} = \sum_{I,J} N_I\left(\mathbf{X}_K\right) M_{KK}^M N_K\left(\mathbf{X}_I\right) \quad \text{or} \quad \mathbf{M} = \mathbf{N}^T\mathbf{M}^M\mathbf{N} \tag{81}$$

The resulting equations can then be solved by explicit or implicit methods.

In the handshake method, the nodes of the two coupled systems are coincident. Therefore the same Lagrangian as in (53) can be used with the constraint term G omitted. Generally, a constant energy scaling function α is used in the overlapping domain, i.e. handshake domain. The overlapping nodes are often coupled with dampers which suppress some of the spurious reflections at the interface.

4.3 Bridging Scale Method

In the bridging scale method as originated in Wagner and Liu [14], the atomic displacements are decomposed into coarse scale and fine scale displacements. The decomposition of the matrix of atomistic displacements is

$$\mathbf{u}_I = \mathbf{N}_{IJ}\mathbf{d}_J^C + \tilde{\mathbf{u}}^A \quad \text{or} \quad \mathbf{u}^A = \underbrace{\mathbf{N}\mathbf{d}^C}_{\bar{\mathbf{u}}} + \tilde{\mathbf{u}}^A \tag{82}$$

where $\bar{\mathbf{u}}$ is the coarse scale field, which as indicated, is usually a finite element continuum field; $\mathbf{d}$ are the nodal displacements of a coarse scale mesh. The notation is the opposite of that in previous sections to conform to [14], so we have added superscripts A and C for atoms and continua, respectively, for clarity.

The key concept in their work is that the coarse scale displacements are obtained by a least square projection weighted by the atomic masses. This projection is

$$\mathbf{d}^C = \mathbf{M}^{-1}\mathbf{M}^A\mathbf{N}\mathbf{u}^A \tag{83}$$

where $\mathbf{M}$ is the matrix of the coarse scale masses, given by

$$\mathbf{M} = \mathbf{N}^T\mathbf{M}^A\mathbf{N} \tag{84}$$

which is the mass that would be obtained by a master-slave relationship, see (81). It can be seen from (83) that the nodal displacements of the finite element mesh can then be obtained at any time from the atomistic displacements.

Combining (82) and (83) gives

$$\mathbf{u}^A = \mathbf{N}\mathbf{M}^{-1}\mathbf{M}^A\mathbf{N}\mathbf{u}^+\tilde{\mathbf{u}}^A = \mathbf{P}\mathbf{u}^A + \tilde{\mathbf{u}}^A \tag{85}$$

$$\mathbf{P} = \mathbf{N}\mathbf{M}^{-1}\mathbf{M}^A\mathbf{N} \tag{86}$$

It follows from the above that

$$\tilde{\mathbf{u}}^A = \left(\mathbf{I} - \mathbf{P}\right)\mathbf{u}^A \tag{87}$$

In the implementation of Wagner and Liu [14] and the subsequent improvements [36, 37], this projection is apparently only used at the interface. By using this concept, they are able to obtain an equation for the fine scale (i.e. relative acceleration) at the interface without any Lagrange multipliers. They use the approach of Adelman and Doll [38].

The approach has been improved and then streamlined by computing the interface nodes by Green's functions for lattices. Green's functions have been developed for various lattices [36, 37]. The method also entails the computation of Fourier transforms at the interface.

To and Li [19] and Li et al. [39] have enhanced the method by joining the coarse-scale to the fine-scale on an overlapping domain by the perfectly matched layer (PML) method. The perfect matched layer method is very efficient in suppressing spurious reflections. Comparisons of the Li-To PML method with the bridging domain method are given in Section 5.

5 Numerical Results

This section describes some models and solutions obtained by concurrent multiscale methods. The first set of examples are for coupling of molecular dynamics with continuum dynamics by the bridging domain method. The second set are coupled QM/MM, QM/CM and QM/MM/CM equilibrium solutions of graphene sheets with a defect.

5.1 Molecular/Continuum Dynamics with Bridging Domain Method

To examine the performance of the bridging domain method, we investigate the reflection and the transmission properties at the molecular-continuum interface. We will also check how well the conservation properties we have proven hold when the equations are integrated numerically. For these purposes, we consider several one- and two-dimensional problems. In all problems, we evaluate the conservation properties by measuring the change of the conserved variable normalized by its initial absolute value, except in the cases where the initial value is zero. For example, for the energy, the error e_{en} is given by

$$e_{en} = \frac{E(t) - E_0}{E_0} \tag{88}$$

where E_0 is the initial energy of the system. In these examples, all of the energy and momentum is imparted to the system by initial conditions in the velocities and displacements. There are no external forces applied. The central difference method (symplectic Verlet) is used for time integration in all examples.

One-dimensional studies. In the first set of examples, we consider a one-dimensional model as shown in Fig. 12. The domain consists of 400 equally spaced atoms with a lattice constant $r_0 = 1.23$, and 400 elements of length $h = n_1 r_0$, so n_1 is the number of bonds in an element. We denote the number of elements in the coupling subdomain by n_2; n_1 and n_2 are varied in the examples to determine the effect of the element size and overlaid domain size on the performance of the bridging domain method. No dummy atom is introduced at the interface between the atomistic and continuum model, because the scaled masses of these atoms vanish according to (59). The motions of these atoms are determined by the compatibility constraints.

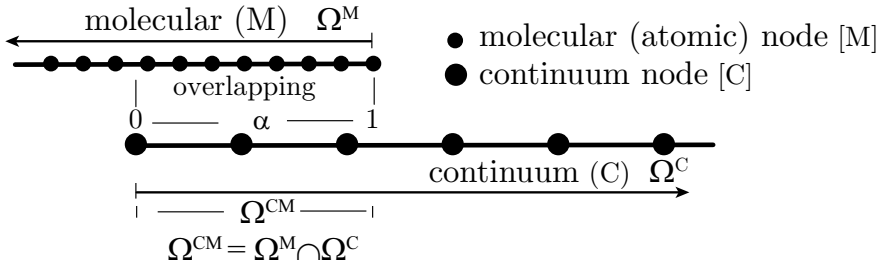

Fig. 12: Schematic of one dimensional coupling model.

The Lennard-Jones potential is chosen to represent the atomic interaction with nearest neighbour assumption.

$$w_{IJ}^{M} = 4\beta_1 \left[\left(\frac{\beta_2}{r_{IJ}} \right)^{12} - \left(\frac{\beta_2}{r_{IJ}} \right)^{6} \right] \tag{89}$$

where $r_{IJ} = \| \mathbf{x}_J - \mathbf{x}_I \|$ is the bond length between the nearest neighboring atoms, i.e. $|I - J| = 1$. β_1 and β_2 are parameters. In these examples, $\beta_1 = 0.2$eV and $\beta_2 = 1.1$. This corresponds to a Young's modulus E_Y =11.66eV/^{3}. The atomic mass $M^M = 1.036 \times 10^{-4}$eV·ps^2/^{2}. The initial displacements and velocities for the atoms with $X \leq 100$ are obtained from linear combinations of the following solutions of the wave equation by letting $t = 0$.

$$u(X,t) = (a_1 + a_1 \cos(2\pi a_2 (X - ct) + \pi))(1 + a_3 \cos(2\pi X)) \tag{90}$$

$$\dot{u}(X,t) = c a_1 \sin(2\pi a_2 (X - ct) + \pi)(1 + a_3 \cos(2\pi X)) \tag{91}$$

$$u(X,0) = \dot{u}(X,0) = 0 \quad \text{for} \quad X > 100 \tag{92}$$

where $c = (E/\rho)^{1/2} = 372.82$/ps is the wave speed, $a_1 = 6.17 \times 10^{-4}$, $a_2 = 0.01$, $a_3 = 0.1$. The initial conditions include waves at four different frequencies $\omega_1 = 2\pi c$, $\omega_2 = 2\pi a_2 c$, $\omega_3 = \omega_1 + \omega_2$, $\omega_4 = \omega_1 - \omega_2$.

Fig. 13 shows the linear momentum as a function of time; we do not use the error measure (88) because the initial momentum is zero. As can be seen, the momentum is exactly conserved until the wave reaches the overlapping subdomain. At that point, there is a moderate fluctuation in the total momentum, but it is restored perfectly after the wave passes. We have no explanation for this temporary violation of momentum conservation.

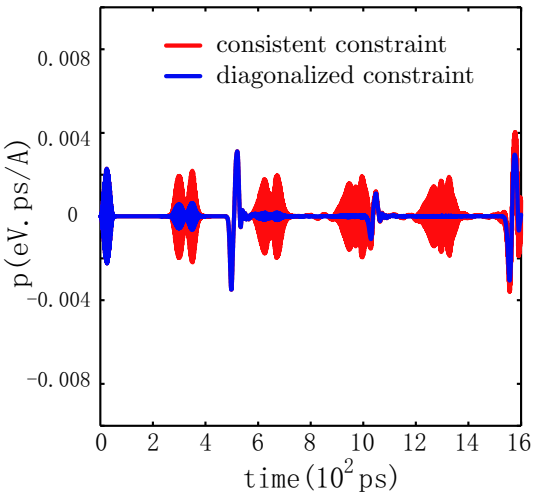

Fig. 13: History of linear momentum of one dimensional coupled model with $n_1 = n_2 = 3$ for consistent and diagonalized constraints methods.

The effectiveness of the bridging domain method can be seen from Fig. 14 which shows the reflection and transmission factors for the interface for various combinations of overlapping elements and atoms per element. In these figures, the cutoff frequencies of the finite element and atomistic models are indicated by vertical lines. The cutoff frequency of the finite element model is given by (49). In the atomistic model, the cutoff frequency is given by $\omega_{\text{cut}}^{M} = (k/m)^{1/2}$, where k is the tangent of the force-elongation curve of the bond; for a Lennard-Jones potential, $k = 36 \times 2^{2/3} \beta_1 / \beta_2^2$. An ideal coupling scheme would suppress all reflections of phonons between the cutoff frequencies of the atomistic model and the continuum model (frequencies above the atomistic frequency are due to aliasing and can be ignored). It is noted that the coupling should transmit all phonons with frequencies below the cutoff frequency of the continuum, so ideally the transmission factor should be unity below the continuum cutoff frequency. Both the diagonalized and consistent constraints show nearly perfect transmission of these phonons. However, the consistent form exhibits substantial reflection of phonons with frequencies between the cutoff frequencies of the atomistic and continuum models. These spurious reflections are far less severe in the diagonalized form.

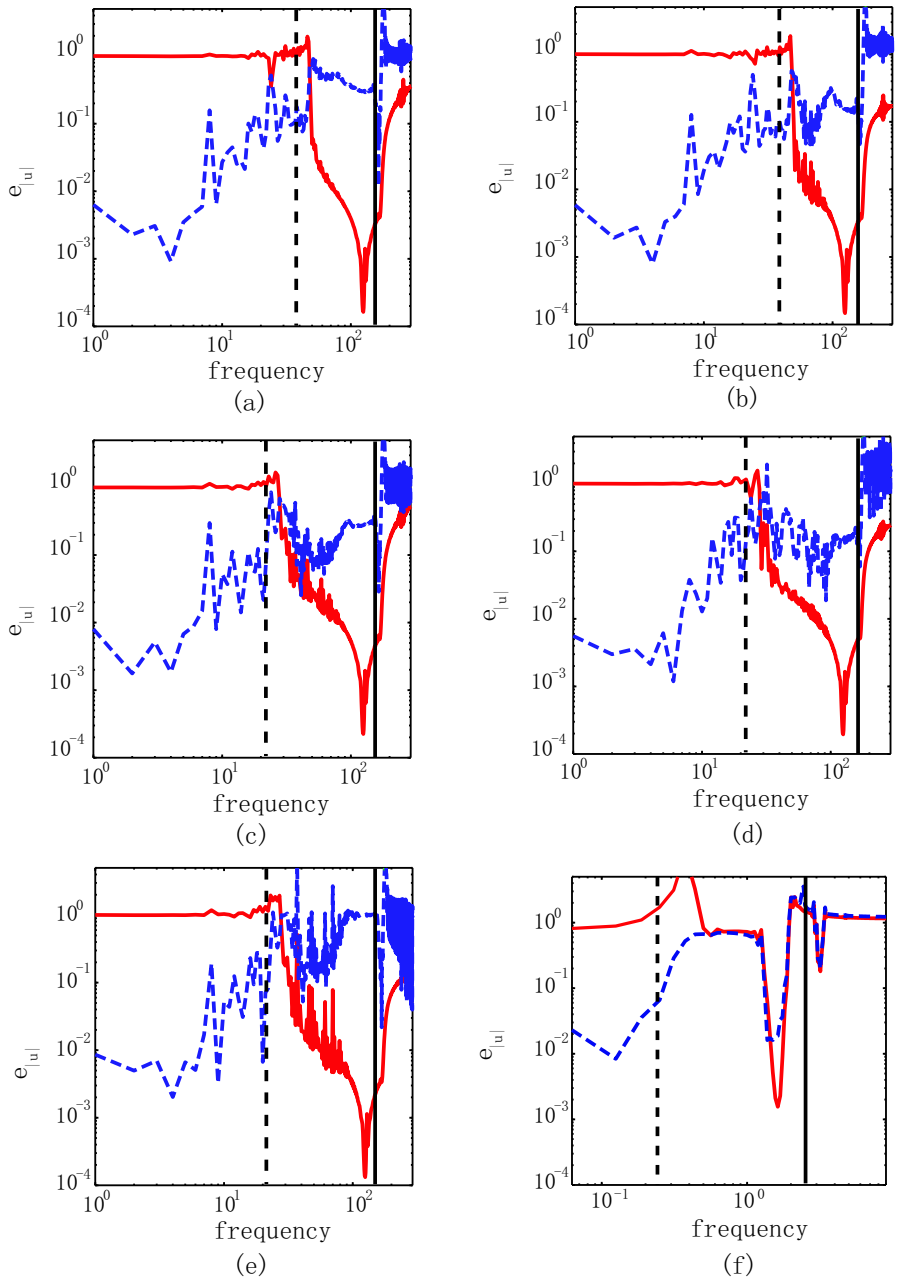

Fig. 14: Reflectivity (blue dashed line) and transmissity (red line) for n_2 overlaid elements with n_1 atoms per element. (a)$n_1 = 4$, $n_2 = 3$, diagonalized constraint; (b)$n_1 = 4$, $n_2 = 6$, diagonalized constraint; (c)$n_1 = 7$, $n_2 = 3$, diagonalized constraint; (d)$n_1 = 7$, $n_2 = 6$, diagonalized constraint; (e)$n_1 = 7$, $n_2 = 3$, consistent constraint; (f) To et al. (20). (The dashed and solid vertical lines are the cutoff frequencies of the continuum and the atomic models, respectively.)

Fig. 14f shows the reflectivity and transmissity of the interface for the To et al. [19] method based on PML. It can be seen that its performance is comparable to that of the bridging domain method with diagonalized constraints.

Table 2 shows the energy dissipation of the high frequency ($\omega > \omega^C_{\text{cut}}$) and the low frequency ($\omega < \omega^C_{\text{cut}}$) incident waves for the diagonalized constraint matrix in one dimension. It is observed that more than 90% of the high frequency energy emanating from the atomistic domain is eliminated, but the low frequency dissipation is less than 1%. The diagonalized constraint matrix damps out the high frequency of the incident wave and effectively eliminates the spurious reflection at the boundary of different scales.

Tab. 2: Energy dissipation of low and high frequency waves for n_1 overlaid elements with $n_2 = 3$

		$n_1 = 7$	$n_1 = 4$
Low	Frequency	0.9%	0.2%
High	Frequency	92%	91%

When the diagonalized constraint matrix is used instead of the consistent constraint matrix, compatibility inside the coupled subdomain is not satisfied exactly. Therefore $\dot{G}$ no longer vanishes, and energy is not conserved. The computations show the time derivative of G is always positive, which implies energy is dissipated when the wave goes through the coupling domain (Fig. 15) according to (78). The amount of energy loss increases as the element size increases relative to the lattice constant.

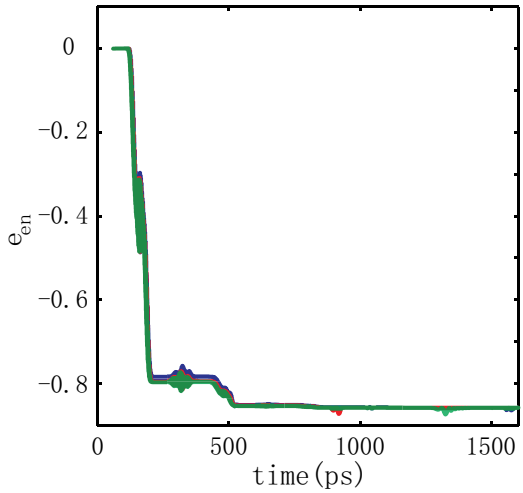

Fig. 15: Error in total energy of coupled model with $n_2 = 3$ (blue), $n_2 = 6$ (red) and $n_2 = 9$ (green) for diagonalized constraints methods.

Two-dimensional studies. In the two-dimensional example, we consider the square lattice (shown in Fig. 16) of 38000 nodes and 40401 atoms. No dummy atoms are introduced at the interface between the atomistic and continuum model for the same reason as in one-dimensional problems. The lattice constants of the atomic model are $r_0 = 1.23\mathring{A}$ and $\theta_0 = 90^o$. Harmonic potentials are used for both stretch and angle bending

$$W^M = \sum_{I\in\mathcal{M}} \sum_{J\in\mathcal{M}>I} \frac{1}{2} k_r (r_{IJ} - r_0)^2 + \sum_L \frac{1}{2} k_\theta (\theta_L - \theta_0)^2 \tag{93}$$

In the above θ_L is the bond angle, $k_r = 14.418\text{eV}/^2$ and $k_\theta = 5.618\text{eV}/$ are the stretch and angle bending constants, respectively, and L is summed over the number of unique three-body interactions. The internal force of atom I, $\mathbf{f}_I^{intM}$, is given by the derivative of the potential function with respect to the atomic coordinates.

$$f_{iI}^{int} = -\frac{\partial W^M}{\partial x_{iI}} = -\sum_{J\in\mathcal{M}} k_r (r_{IJ} - r_0) \frac{\partial r_{IJ}}{\partial x_{iI}} - \sum_L k_\theta (\theta_L - \theta_0) \frac{\partial \theta_L}{\partial x_{iI}} \tag{94}$$

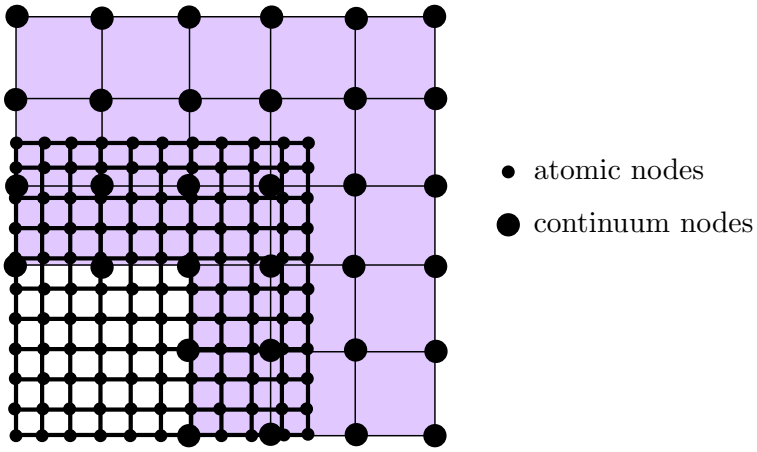

Fig. 16: Schematic of two dimensional coupled model (in calculations, more elements and nodes were used).

We consider the model shown in Fig. 16; four-fold symmetry is used. We initiate a cylindrical wave at the bottom left in the atomistic model with the initial conditions

$$\begin{aligned} u_1(\mathbf{X}_I) &= \big[a_1 + a_1\cos(2\pi a_2 r_I + \pi)\big]\big[1 + a_3\cos(2\pi r_I)\big]\cos\gamma \\ u_2(\mathbf{X}_I) &= \big[a_1 + a_1\cos(2\pi a_2 r_I + \pi)\big]\big[1 + a_3\cos(2\pi r_I)\big]\sin\gamma \\ \dot{u}_1(\mathbf{X}_I) &= 2\pi c a_1\sin(2\pi a_2 r_I + \pi)\big[1 + a_3\cos(2\pi r_I)\big]\cos\gamma \\ \dot{u}_2(\mathbf{X}_I) &= 2\pi c a_1\sin(2\pi a_2 r_I + \pi)\big[1 + a_3\cos(2\pi r_I)\big]\sin\gamma \end{aligned} \tag{95}$$

for the atoms with $r_I \leq 100$, where $r_I = ||\mathbf{x}_I||$ is the distance of atom I to the origin, and γ is the angle between the positive x direction and $\mathbf{x}_I$. The initial displacements and velocities vanish for the rest of the atoms. The values of a_1, a_2 and a_3 are the same as in the one-dimensional examples. The incident wave contains four different frequencies ω_1 to ω_4.

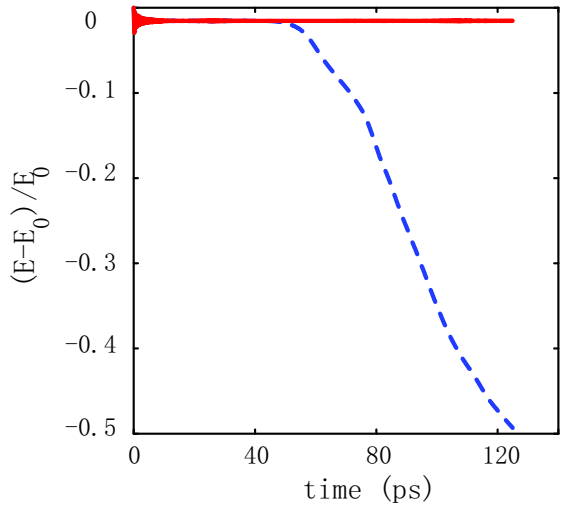

Fig. 17: Rate change in total energy for two dimensional example with consistent (solid line) and diagonalized (dashed line) constraints ($n_1 = 4$, $n_2 = 1$).

The linear momentum of the system is perfectly conserved for both the consistent and diagonalized constraints. There is no temporary loss of linear momentum as observed in the one-dimensional examples when the wave reaches the overlapping domain. The initial total angular momentum is zero, and remains so when using the consistent constraint. For the diagonalized constraint, the angular momentum in the coupling domain oscillates about zero with an amplitude of 10^{-3}.

The error in energy is shown in Fig. 17. The energy is conserved with the consistent constraint. For the diagonalized constraint, about 45% of the energy is dissipated after the waves passes the coupling domain; most of this energy is in the high frequency part of the spectrum.

5.2 Fracture of Defected Graphene Sheets by QM/MM and QM/CM Methods

Here we describe coupled QM/MM and QM/CM calculations of defected graphene sheets. The coupled method uses the modified Tersoff-Brenner (MTB-G2) potential for the molecular mechanics model and a linear elastic finite element model for continuum mechanics. The quantum mechanics calculations were made with the semi-empirical method PM3 [41]. MTB-G2 [42, 43, 44, 45] is a modified version of the standard reactive empirical bond order (REBO) [44] potential, in which the cutoff function is removed and interatomic interactions are included only for those atom pairs that are less than 2.0 Å apart in the initial unstrained configuration. This was found [42, 45] to be necessary to prevent spuriously high values of the fracture strength due to the cutoff function.

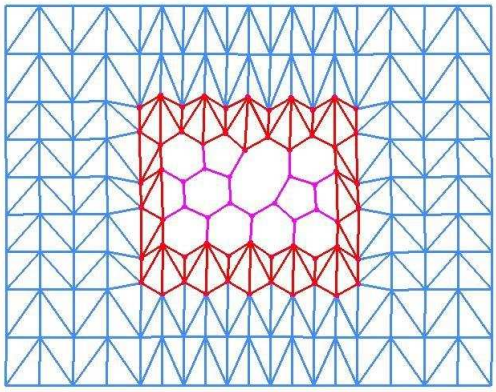

Fig. 18: A QM/CM model of a graphene sheet containing an asymmetric two-atom vacancy defect. Pink (light, ball and stick) atoms in the center constitute the strictly QM region, red (dark, ball and stick) atoms constitute the overlapping region, and blue (light, stick) region represents the strictly CM region.

Three coupling methods were used to calculate the stress-strain curves and fracture stresses of a graphene sheet containing defects. In these calculations, the end carbon atoms of the graphene sheet were displaced with increments of 0.5% of the sheet length until the sheet fractures. At each strain increment, the atomistic configuration was optimized with the carbon atoms at each edge constrained to lie within a plane. Once the geometry was optimized at a given applied strain, the tensile stress in the sheet was calculated by taking derivatives of the energy using finite differences with respect to the strain. An effective thickness of 3.4 Å was used for the stress calculations; this corresponds to the interlayer spacing in graphite, and is widely used for stresses on graphene sheets.

We first consider a graphene sheet containing an asymmetric two-atom vacancy [46, 47]. It was stretched in the direction perpendicular to the zigzag edge. The coupled models of this system for the three coupling methods considered are shown in Figs. 18-19. The sheet was 27 Å by 21 Å and contained 248 carbon atoms with 64 carbon atoms in the QM domain and 38 carbon atoms in the overlapping domain for the modified ONIOM (called QtMMOD) scheme, see [30]. The results were compared to those calculated by pure QM calculations. In addition to the two QM/MM models, a QM/CM model (shown in Fig. 18) using triangular elements was also used.

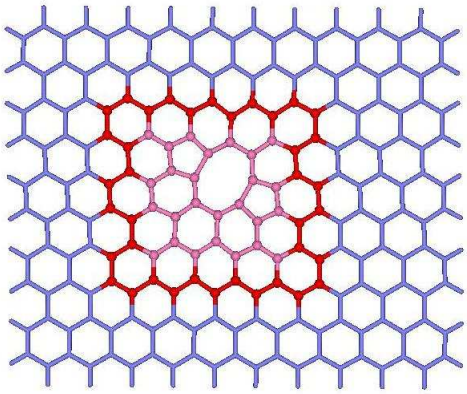

Fig. 19: A QtMMOD model of a graphene sheet containing an asymmetric two-atom vacancy defect. Pink (light, ball and stick) atoms constitute the strictly QM region, red (dark, ball and stick) atoms constitute the overlapping region, and blue (light, stick) atoms constitute the strictly MM region.

The stress-strain curves for the three methods are shown in Fig. 20. The stresses calculated by the QtMMOD and ONIOM coupling methods are almost indistinguishable. Both results match quite well with the benchmark pure QM results although there are small differences near the fracture strain. The QtMMOD and ONIOM methods calculated fracture stress values of 87.4 GPa and 87.2 GPa, respectively, in comparison to 88.1 GPa obtained from the strictly QM calculations. The stress-strain curve for the QM/CM coupled calculations matches the stresses from the other methods quite well and yields a fracture stress value of 87.3 GPa. However, small differences are observed, which may be due to several reasons, such as the fact that a finite element model does not reflect the physics near the defect as accurately as the MM method. Nevertheless, the QM/CM model is still sufficiently accurate to be useful for studies of large systems, such as calculations of the fracture stress of a graphene sheet containing a crack [1]. In such models, the region near the crack tip can be modeled quantum mechanically and the CM model can be applied elsewhere.

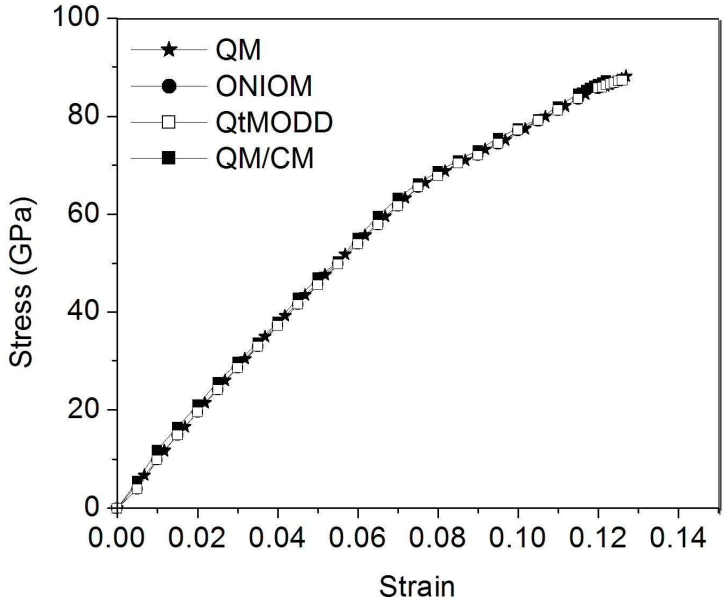

Fig. 20: Stress-strain curves obtained by the ONIOM, QtMMOD, QM/CM coupling, and pure QM methods for the graphene sheet models shown in Figs. 3-5.

Fig. 22 shows the comparison of elasticity solution of the strain ϵ_y at stress intensity factor K = 3 MPa$\sqrt{\text{m}}$ with the results calculated by the QM/MM methods. The strains were computed from the configuration by the MLS scheme [48, 49]. The agreement is quite good, although the atomistic strains are not as localized near the crack tip as in the elastic solution.

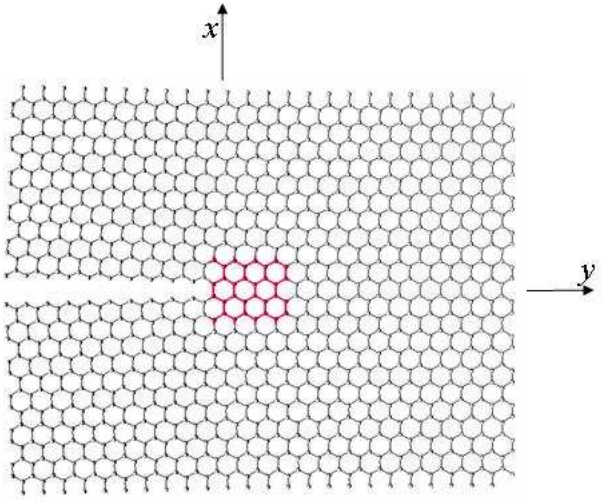

Fig. 21: QM/MM model of a graphene sheet with a crack. Red (dark) atoms represent the QM subdomain and the Grey (light) atoms represent additional atoms treated at the MM level.

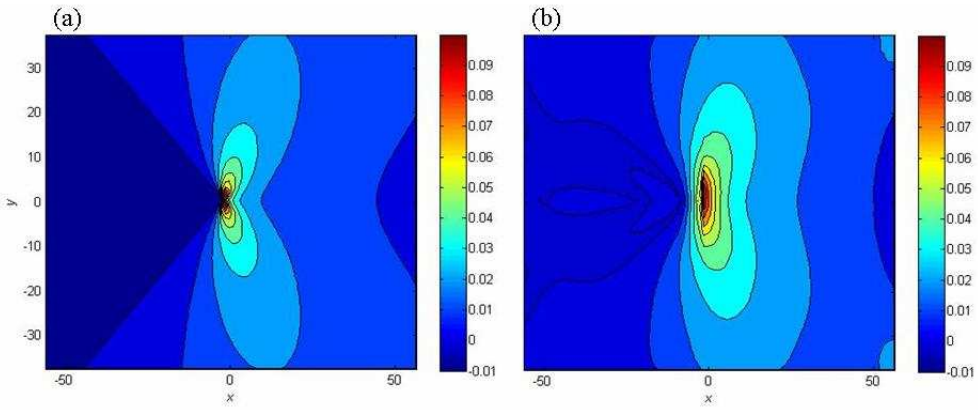

Fig. 22: ϵ_y obtained from (a) elasticity solution and (b) MLS method for the sheet shown in Fig. 21

Crack propagation in graphene sheet: comparison with Griffith's formula. In this example we consider the fracture strength of a graphene sheet with slit defects of various lengths and compare the calculated strengths to those predicted by Griffith's formula for a crack in an infinite sheet. Slit defects were created by removing four rows of atoms and then saturating the dangling bonds by hydrogen atoms [1, 43]. In order to be able to compare with the results for an infinite sheet, very large sheets were required, so we used a QM/MM/CM concurrent calculation [2], where the QM/MM coupling was obtained by using the modified ONIOM scheme and the bridging domain method was used to link the MM model to a finite element model. The PM3 method [41] was used for the quantum calculation.

A representation of the QM/MM/CM model for one slit size is shown in Fig. 23. The dimensions of the full sheet are 393.5 Å by 411.8 Å, the QM model consists of 76 atoms around the slit. The atomistic region is 115.5 Å by 82.3 Å and located in the center of the sheet.

In Fig. 96 the numerical results are compared with the results of the Griffith formula, which is given by

$$\sigma = \sqrt{\frac{2Y\gamma}{\pi a}}, \tag{96}$$

where σ is the Griffith formula stress, Y is the Young's modulus, a is the half length of the slit, and γ is the surface energy density. We calculated γ as the difference between the PM3 energy of a geometry optimized pristine square sheet and the energy of the two fragments after they are separated to a large distance, and subsequently optimized to yield their equilibrium geometries, divided by twice the surface area. The factor of two is included because two surfaces are produced by fracture.

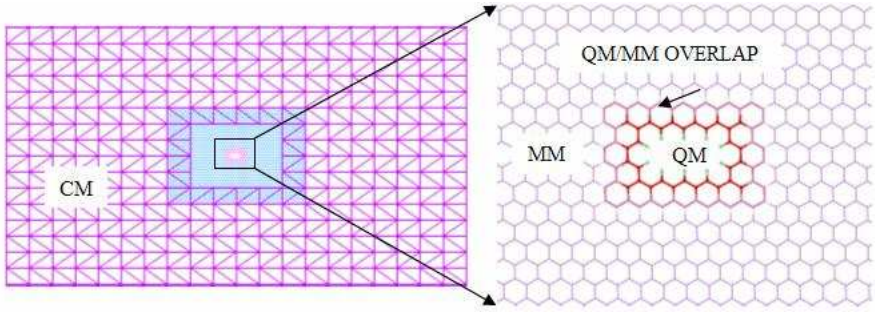

Fig. 23: QM/MM/CM model of a graphene sheet containing a slit-like defect.

The QM/MM/CM results agree well with the prediction of the Griffith formula and decrease approximately as the inverse of the square root of the crack length. The Griffith stress is a lower bound on the fracture stress, but

the approximate stress estimates of the Griffith formula need not be, and as seen in Fig. 24, the Griffith formula results fall below the numerical ones for slits longer than 20 Å. Note that on the whole, remarkably good agreement is obtained between the Griffith formula and the QM/CM/MM calculation, which indicates that the Griffith formula is also applicable to nanoscale fracture.

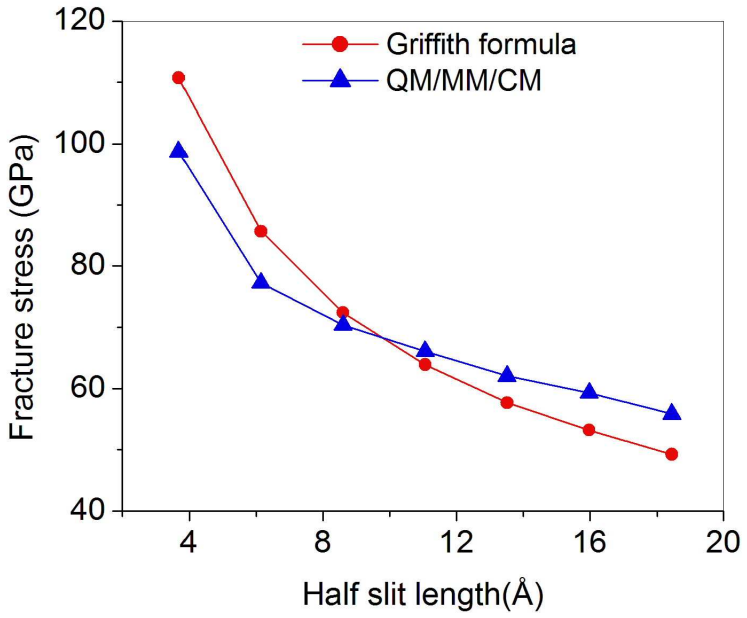

Fig. 24: Results of the Griffith formula versus QM/MM/CM fracture strengths for a graphene sheet containing a slit-like defect.

References

[1] Khare, R., Mielke, S.L., Paci, J.T., Zhiang, S., Ballarini, R., Schatz, G.C. and Belytschko, T. (2007). Coupled quantum mechanical/molecular mechanical modeling of the fracture of defective carbon nanotubes and graphene sheets. *Phys. Rev. B* , **75**, 075412.

[2] Khare, R., Mielke, S.L., Schatz, G.C. and Belytschko, T. (2008). Multiscale coupling schemes spanning the quantum mechanical, atomistic forcefield, and continuum regimes. *Comput. Methods Appl. Mech. Engrg*, in press.

[3] Baskes M.I., Melius C.F., and Wilson, W.D. (1980). Solubility and Diffusivity of Hydrogen and Helium at Dislocations and in the Stress Field Near a Crack Tip. *Interatomic Potentials and Crystalline Defects*, 249–271.

[4] Mullins, M., and Dokainish, M.A. (1982). Simulation of the (001) plane crack in α-iron employing a new boundary scheme. *Phil. Mag. A*, **46**, 771–787.

[5] Belytschko, T., Liu, W.K., and Moran, B. (2001) *Nonlinear Finite Elements for Continua and Structures*, John Wiley & Sons Inc.

[6] Kohlhoff, S., Gumbsch, P., and Fischmeister, H.F. (1991). Crack propagation in bcc crystals studied with a combined finite-element and atomistic model. *Phil. Mag. A*, **64**, 851–878.

[7] Shilkrot, L.E., Curtin, W.A., and Miller, R.E. (2002). A coupled atomistic/continuum model of defects in solids. *J. Mech. Phys. Solids*, **50**, 2085–2106.

[8] Tadmor, E.B., Ortiz, M., and Phillips, R. (1996). Quasicontinuum analysis of defects in solids. *Phil. Mag. A*, **73**, 1529–1563.

[9] Shenoy, V.B., Miller, R., Tadmor, E.B., Rodney, D., Phillips, R., and Ortiz, M. (1998). An adaptive methodology for atomic scale mechanics: the quasicontinuum method. *J. Mech. Phys. Solids*, **47**, 611–642.

[10] Knap, J., and Ortiz, M. (2001). An analysis of the quasicontinuum method. *J. Mech. Phys. Sol.*, **49**, 1899–1923.

[11] Rudd, R.E., and Broughton, J.Q. (1998). Coarse-grained molecular dynamics and the atomic limit of finite elements. *Phys. Rev. B*, **58**, R5893-R5896.

[12] Abraham, F.F., Broughton, J.Q., Bernstein, N., and Kaxiras, E. (1998). Spanning the length scales in dynamic simulation. *Computers in Physics*, **12**, 538–546.

[13] Broughton, J.Q., Abraham, F.F., Bernstein, N., and Kaxiras, E. (1999). Concurrent coupling of length scales: methodology and application. *Phys. Rev. B*, **60**, 2391–2403.

[14] Wagner, G. J., and Liu, W.K. (2003). Coupling of atomistic and continuum simulations using a bridging scale decomposition. *Journal of Computational Physics*, **190**, 249–274.

[15] Song, J.-H., Loehnert, S. and Belytschko, T. (2008). Multi-scale Aggregating Discontinuities: A method for Circumventing Loss of Material Stability. *Int. J. Numer. Mech. Engng*, **73**, 869–894.

[16] Farrell, D.E., Park, H.S., and Liu, W.K. (2007). Implementation aspects of the bridging scale method and application to intersonic crack propagation. *Int. J. Numer. Meth. Engng.*, **71**, 583–605.

[17] Cai, W., Koning, M., Bulatov, V.V., and Yip, S. (2000). Minimizing boundary reflections in coupled-domain simulation. *Phys. Rev. Lett.*, **85**, 3213–3216.

[18] E, W., Huang, Z. (2001). Matching conditions in atomistic-continuum modeling of materials. *Phys. Rev. Lett.*, **87**, 135501.

[19] To, A., and Li, S.F. (2005). Perfectly matched multiscale simulations. *Phys. Rev. B*, **72**, 035414.

[20] Berenger, J.P. (1994). A perfectly matched layer for the absorption of electromagnetic waves. *J. Comput. Phys.*, **114**, 185–200.

[21] Xiao, S.P., and Belytschko, T. (2004). A bridging domain method for coupling continua with molecular dynamics. *Comput. Meth. Appl. Mech. Eng.*, **193**, 1645–1669.

[22] Belytschko, T., and Xiao, S.P. (2003). Coupling methods for continuum model with molecular model. *Int. J. Numer. Meth. Engng.*, **1**, 115–126.

[23] Guidault, P.A., and Belytschko, T. (2007). On the L^2 and the H^1 couplings for an overlapping domain decomposition method using Lagrange multipliers. *Int. J. Numer. Meth. Engng*, **70**, 322–350.

[24] Fish, J., Nuggehally, M.A., Shephard, M.S., Picu, C.R., Badia, S., Parks, M.L., Gunzburger, M. (2007). Concurrent AtC coupling based on a blend of the continuum stress and the atomistic force. *Comput. Methods Appl. Mech. Engrg.*, **196**, 4548–4560.

[25] Li, X., and E, W. (2005). Multiscale modeling of the dynamics of solids at finite temperature. *J. Mech. Phys. Solids*, **53**, 1650–1685.

[26] Dhia, H.B., and Rateau, G. (2001). Mathematical analysis of the mixed Arlequin method. *Comptes Rendus de l'Academie des Sciences Series I Mathematics*, **332**, 649–654.

[27] Dhia, H.B., and Rateau, G. (2005). The Arlequin method as a flexible engineering desing tool. *Int. J. Numer. Mech. Engng.*, **62**, 1442–1462.

[28] Feyel, F., and Chaboche, J.L. (2000). FE^2 multiscale approach for modelling the elastoviscoplasitic behavior of long fibre SiC/Ti composite materials. *Comput. Methods Appl. Mech. Engrg.*, **183**, 309–330.

[29] Kouznetsova, V., Brekelmans, W.A.M., and Baaijens, F.P.T. (2001). An approach to micro-macro modeling of heterogeneous materials. *Computational Mechanics*, **27**, 37–48.

[30] Zhang S., Khare, R., Lu, Q. and Belytschko, T. (2007). A bridging domain and strain computation method for coupled atomistic/continuum modelling of solids. *Int. J. Numer. Mech. Engng.*, **70**, 913–933.

[31] Curtin W.A., and Miller R.E. (2003). Atomistic/continuum coupling in computational materials science. *Modelling and Simulation in Materials Science and Engineering*, **11**, R33–R68.

[32] Svensson, M., Humbel, S., Froese, R.D.J., Matsubara, T. Sieber, S., and Morokuma, K. (1996). ONIOM: a multilayered integrated MO+MM method for geometry optimizations and single point energy predictions. A test for Diels-Alder reactions and $Pt(P(t\text{-}Bu)_3)_2+H_2$ oxidative addition. *J. Phys. Chem.*, **100**, 19357–19363.

[33] Xu, M., and Belytschko, T. (2008). Conservation properties of the bridging domain method for coupled molecular/continuum dynamics. *Int. J. Numer. Meth. Engng.*, in press.

[34] Hairer, E., Norsett, S.P., and Wanner, G. (2002). *Solving ordinary differential equations*, Springer.

[35] Belytschko, T., Krongauz, Y., Dolbow, J., and Gerlach, C. (1998). On the completeness of meshfree particle methods. *Int. J. Numer. Mech. Engng.*, **43**, 785–819.

[36] Karpov, E.G., Wagner, G.J., and Liu, W.K. (2005). A Green's function approach to deriving non-reflecting boundary conditions in molecular dynamics simulation. *Int. J. Numer. Mech. Engng.*, **62**, 1250–1262.

[37] Park, H.S., Karpov, E.G., Klein, P.A., and Liu, W.K. (2005). The bridging scale for two-dimensional atomistic/continuum coupling. *Philosophical Magazine*, **85**, 79–113.

[38] Adelman, S.A., and Doll, J.D. (1974). Generalized langevin equation approach for atom/solid-surface scattering-collinear atom/harmonic chain model. *J. Chem. Phys.*, **61**, 4242–4245.

[39] Li, S., Liu, X., Agrawal, A., and To, A. (2006). Perfectly matched multiscale simulations for discrete lattice systems: Extension to multiple dimensions. *Phys. Rev. B*, **74**, 045418.

[40] Khare R., Mielke S.L., Paci J.T., Zhang S., Ballarini R., Schatz G.C., Belytschko T. (2007). Coupled quantum mechanical/molecular mechanical modeling of the fracture of defective carbon nanotubes and graphene sheets. *Phys. Rev. B*, **75**, 75412.

[41] Stewart, J.J.P. (1989). Optimization of Parameters for Semiempirical Methods. *J. Comput. Chem.*, **10**, 209–220.

[42] Belytschko, T., Xiao, S.P., Schatz, G.C., and Ruoff, R.S. (2002). Atomistic simulations of nanotube fracture. *Phys. Rev. B*, **65**, 235430.

[43] Zhang, S., Mielke, S.L., Khare, R., Troya, D., Ruoff, R.S., Schatz, G.C., and Belytschko, T. (2005). Mechanics of defects in carbon nanotubes: Atomistic and multiscale simulations. *Phys. Rev. B*, **71**, 115403.

[44] Brenner, D.W., Shenderova, O.A., Harrison, J.A., Stuart, S.J., Ni, B. and Sinnott, B. (2002). A second-generation reactive empirical bond order (REBO) potential energy expression for hydrocarbons. *J. Phys.: Condens. Matter*, **14**, 783–802.

[45] Shenderova, O.A., Brenner, D.W., Omeltchenko, A., Su, X., and Yang, L.H. (2000). Atomistic modeling of the fracture of polycrystalline diamond. *Phys. Rev. B*, **61**, 3877–3888.

[46] Mielke, S.L., Troya, D., Zhang, S., Li, J.L., Xiao, S.P., Car, R., Ruoff, R.S., Schatz, G.C., and Belytschko, T. (2004). The role of vacancy defects and holes in the fracture of carbon nanotubes. *Chemical Physics Letters*, **390**, 413–420.

[47] Krasheninnikov, A.V., Nordlund, K., Sirvio, M., Salonen, E., and Keinonen, J. (2001). Formation of ion-irradiation-induced atomic-scale defects o walls of carbon nanotubes. *Phys. Rev. B*, **63**, 245405.

[48] Belytschko, T., Lu, Y.Y., and Gu, L. (1994). Element-free Galerkin methods. *Int. J. Numer. Mech. Engng.*, **37**, 229–256.

[49] Belytschko, T., Krongauz, Y., Organ, D., Fleming, M., and Krysl, P. (1996). Meshless methods: An overview and recent developments. *Comput. Methods Appl. Mech. Engrg.*, **139**, 3–47.